https://doi.org/10.5194/egusphere-2026-1800
Preprint. Discussion started: 18 May 2026

Radar-Derived Intensity-Duration-Area-Frequency Relations for Assessing Hydrological Hazards in Complex Terrain

Talia Rosin[1], Francesco Marra[2], Marco Gabella[3], Urs Germann[3], Daniel Wolfensberger[3], Efrat Morin[1]

[1]The Fredy and Nadine Herrmann Institute of Earth Sciences, the Hebrew University of Jerusalem, Jerusalem, 9190401, Israel
[2]Department of Geosciences, University of Padova, Italy
[3]Federal Office of Meteorology and Climatology MeteoSwiss, Locarno-Monti, Switzerland

Correspondence to: Talia Rosin (talia.rosin@mail.huji.ac.il), Efrat Morin (efrat.morin@mail.huji.ac.il)

Abstract. Extreme rainfall in complex terrain is highly variable across space and time, challenging accurate estimation of design-relevant return levels. While rain gauge networks provide precise point measurements, their sparse distribution limits their ability to characterise this fine-scale variability and assess areal precipitation amounts. Weather radar offers the spatial coverage and temporal resolution required.

In this study we leverage 9 years (2016–2024) of summer (June-August) precipitation data from the Swiss five radar, dual-polarisation C-band network (1 km, 5 min) to quantify summer precipitation extremes over Switzerland across durations from 30 min to 24 h and spatial aggregations from 1 to 500 km^2. Return levels are estimated using the Simplified Metastatistical Extreme Value (SMEV) framework, which is well-suited to short, error-prone records, and validated against corresponding estimates from 60 long-term quality-controlled rain gauges. The resulting Intensity–Duration–Area–Frequency (IDAF) relationships explicitly capture how extremes vary jointly across space and time.

Rainfall extremes exhibit a pronounced dependence on spatiotemporal scale, and vary spatially depending on the large-scale flows typical of the region and its topographic structure. For short durations and small areas, the largest return levels are concentrated in regions where strong orographic lifting is expected, including the Jura and north- and south-Alpine windward slopes, while lower values occur over the Plateau and inner Alpine valleys. As duration and area increase, small-scale peaks are progressively smoothed, and broader regions of high intensity return levels emerge, with the Southern Alps remaining a consistent hotspot across all scales. Analysis of three recent high-impact flood-producing storms illustrates how the spatiotemporal distribution of rainfall governs hydrological hazard, and how radar can capture localised extremes often missed by gauges.

Overall, the resulting multiscale return level maps provide an improved basis for hydrological design and risk assessment in complex terrain, demonstrating the value of radar-based IDAF analysis and the ability of the framework to derive scale-aware flood-relevant extremes from short radar records.

https://doi.org/10.5194/egusphere-2026-1800
Preprint. Discussion started: 18 May 2026

1 Introduction

Extreme rainfall events trigger a range of severe natural hazards, including floods, flash floods, debris flows, and landslides, with substantial social and economic consequences. In complex Alpine terrain such as Switzerland, the interaction between atmospheric processes and heterogeneous topography amplifies these hazards.

A major challenge in flood prediction and hazard assessment arises from the pronounced scale dependency of rainfall extremes, whereby precipitation intensity, duration, and spatial organisation vary across orders of magnitude in space and time, reflecting the multi-scale interplay of atmospheric processes (Borga et al., 2014; Caldas-Alvarez et al., 2022). Hydrological response depends on both rainfall spatiotemporal variability and catchment properties. Rainfall extremes for durations close to a catchment's time of concentration are more likely to generate extreme streamflow responses (Blöschl & Sivapalan, 1997). Consequently, small catchments are particularly susceptible to local, high-intensity convective storms, while larger basins typically flood under long-duration, widespread rainfall, often enhanced by antecedent soil moisture or snowmelt (Beven, 2012; Blöschl & Sivapalan, 1997; Tarasova et al., 2018). A scale-aware understanding of how extreme precipitation interacts with catchments across space-time scales, and the associated probabilities of occurrence, is therefore essential for robust hydrological hazard assessment and prediction.

Accurately characterising rainfall extremes is, however, inherently challenging. Such events are rare and highly variable in space and time. Rain gauge networks are often too sparse to represent localised extremes and can suffer from representativeness errors (Karklinsky & Morin, 2006; Ochoa-Rodriguez et al., 2015; Thomassen et al., 2022). Even dense networks often struggle to capture the full fine-scale spatial structure of precipitation (Gires et al., 2014; Lengfeld et al., 2020; Villarini et al., 2008), a critical limitation for urban and mountainous hydrology with short catchment response times (Ochoa-Rodriguez et al., 2015). In complex terrain, additional challenges arise: gauges are frequently located in accessible valley sites near roads and settlements rather than on steep slopes or mountain crests, contributing to uneven spatial coverage across elevations and systematic sampling bias. At high altitudes, strong winds and frequent solid precipitation further exacerbate measurement errors through severe undercatch, resulting in systematic underestimation of precipitation (Muchan & Dixon, 2019). Consequently, reliably quantifying elevation-dependent gradients in precipitation from gauge observations alone remains inherently challenging.

Weather radar provides the spatial coverage and temporal resolution needed to accurately analyse rainfall down to kilometre and sub-hourly resolutions (Berne et al., 2004; Cristiano et al., 2017; Thorndahl et al., 2017). Despite uncertainties related to ground clutter, bright-band contamination, mixed-phase precipitation, and the variability of the reflectivity-rain rate (Z–R) relationship, advances in radar processing in recent years have significantly improved quantitative precipitation estimation (QPE).

Extreme precipitation has traditionally been analysed using asymptotic approaches based on extreme value theory. These include block maxima methods, where annual or seasonal maxima of asymptotically large blocks can only converge to the Generalised Extreme Value (GEV) distribution, and threshold exceedance methods, where Poisson exceedances of an

https://doi.org/10.5194/egusphere-2026-1800
Preprint. Discussion started: 18 May 2026

asymptotically high threshold can only converge to the Generalised Pareto distribution (Coles, 2001). Both approaches utilise a small subset of available data and thus require long observational records, typically obtainable only from gauge networks. In addition, these approaches heavily rely on asymptotic assumptions, which are likely not met in the case of precipitation (Marra et al., 2023, 2026).

More recent non-asymptotic approaches include the Metastatistical Extreme Value (MEV) framework (Marani & Ignaccolo, 2015) and its simplified variant, the SMEV (Marra et al., 2019), which estimate extreme value distributions from the bulk distribution of 'ordinary' events rather than from extremes only, without resorting to asymptotic assumptions. This reduces parameter uncertainty and enables reliable estimation of rare return levels from short or error-prone records, making them particularly well-suited for short radar archives (Marra et al., 2018; Zorzetto et al., 2016). The SMEV framework has been successfully applied to both point-based and spatial precipitation datasets worldwide, consistently showing improved performance over GEV-based models, especially when applied to short records (Vidrio-Sahagún & He, 2022). In particular, records of approximately 10 years have been shown to be sufficient for deriving stable return level estimates using the SMEV framework (Marra et al., 2022; Rosin et al., 2024).

Recently, Rosin et al. (2024) extended the SMEV framework to the areal scale, using 12 years of radar-derived precipitation data over the Eastern Mediterranean to estimate return levels across multiple spatiotemporal scales. The study showed that short radar records can be used to reliably incorporate spatial aggregation into extreme rainfall analysis and to drive Intensity–Duration–Area–Frequency (IDAF) relationships at high spatial resolution. Here, we further advance this framework by applying the areal SMEV to the complex and heterogeneous Alpine topography of Switzerland, and by explicitly linking duration–area scaling of extreme rainfall to observed impacts.

Previous studies have examined Swiss precipitation extremes using gauge data at daily (Frei & Schär, 1998; Haruna et al., 2022, 2025; Isotta et al., 2014) and sub-daily accumulations (Haruna et al., 2023). Studies utilising radar data have provided valuable insights into the spatial variability of extremes (Barton et al., 2016; Wüest et al., 2010). Recent works utilise the blended CombiPrecip radar–gauge dataset to quantify extremes at point (Barton et al., 2020; Panziera et al., 2016, 2018) and areal (Haruna et al., 2024) scales, demonstrating pronounced duration-dependent spatial patterns. Benoit et al. (2024) highlighted the role of topography in shaping precipitation climatology using combined radar-gauge data. While these studies have substantially advanced our understanding of Swiss precipitation, they focus predominantly on point-scale or fixed-grid analyses, which cannot account for the spatial footprint of storms, and therefore cannot directly provide the intensity–duration–area relationships required for hydrological design and hazard assessment.

Using nine years (2016–2024) of summer (June–August) radar-derived precipitation data over Switzerland, we estimate multiscale return levels for durations from 30 min to 24 h and aggregation areas from 1 to 500 km², for return periods up to 100 years. Although short, this record length is sufficient to derive stable extreme-value estimates using the SMEV framework, as demonstrated in previous studies (Dallan et al., 2024; Marra et al., 2022; Rosin et al., 2024), which showed that using SMEV on such short radar records provided more accurate estimates than the ones obtained using traditional GEV approaches on the full rain gauge records. The resulting IDAF fields are evaluated against long-term rain gauge records and used to analyse three

https://doi.org/10.5194/egusphere-2026-1800
Preprint. Discussion started: 18 May 2026

recent high-impact flood events, including the July 2021 regional floods and the June 2024 event, to demonstrate how hydrological hazard shifts with the spatiotemporal structure of precipitation extremes.

The remainder of this article is organised as follows: Section 2 presents the study area and datasets, Section 3 describes the methodology, Section 4 presents the results; Section 5 analyses the three extreme flood events. Finally, Section 6 discusses the influence of location and elevation on rainfall intensity, and how this is affected by space and time scale.

2 Study area and data

We consider a domain of 240×360 km^2, centred on and surrounding Switzerland (Fig. 1). The region is characterised by highly diverse and complex topography, ranging from low-elevation forelands to steep Alpine terrain, which creates pronounced spatial gradients and significant seasonal, regional and scale-dependent variations in average and extreme precipitation (Barton et al., 2020; Giannakaki & Martius, 2016; Isotta et al., 2014).

From a geographical and climatological perspective, the area can be divided into six hydrometeorologically distinct sub-regions (Fig. 1b): the Jura mountains, Plateau, Pre-Alps, Western Alps and Eastern Alps (together the Central Alps), and Southern Alps (Barton et al., 2020; Frei & Schär, 1998; Molnar & Burlando, 2008). The Alpine massif serves as a primary climatic divider. North of the Alps, a central European weather regime predominates, with orographic enhancement driving high rainfall across the Jura and Pre-Alps, while the sheltered Plateau remains comparatively drier. Conversely, the inner-Alpine valleys in the Central Alps lie in persistent rain shadows, experiencing the driest conditions. The Southern Alps are influenced by Mediterranean moisture transport and significant orographic lift, resulting in the highest accumulations and most

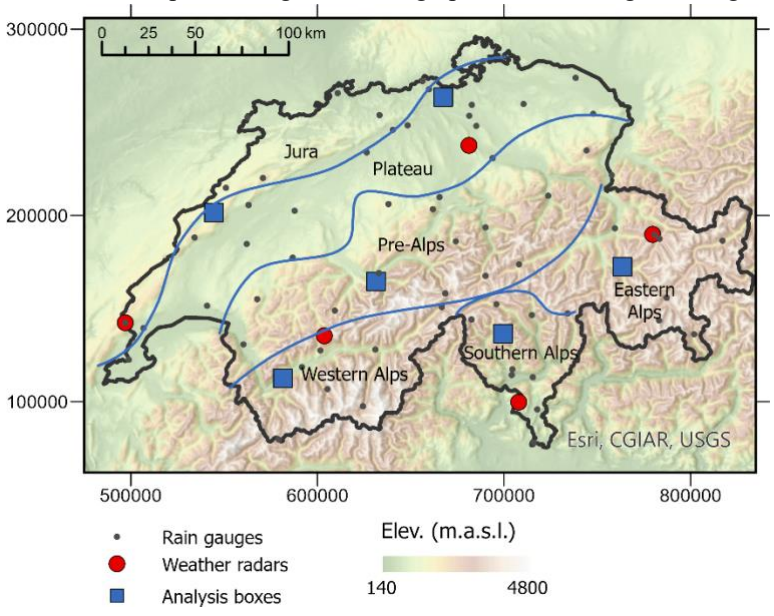

Figure 1. Geographical map of the study area, displaying six topographical regions (Jura Mountains, Swiss Plateau, Pre-Alps, Eastern Alps, Western Alps and Southern Alps). Blue squares indicate the six regional analysis boxes used in Fig. 6. Basemap sources: Esri, CGIAR, USGS | Powered by Esri.

https://doi.org/10.5194/egusphere-2026-1800
Preprint. Discussion started: 18 May 2026

intense rainfall. Annual precipitation exceeds 2,000 mm in the Pre-Alps, Jura, and Southern Alps, while the inner-Alpine valleys receive 400–800 mm (Isotta et al., 2014).

2.1 Radar data

Radar-derived QPE data at 5 min and 1 km^2 resolution (Cartesian plane) are obtained from five dual-polarisation Doppler C-band radars operated by MeteoSwiss, located at altitudes from 900 to 2900 m.a.s.l. (Fig. 1a).

The orographic complexity of Switzerland imposes significant technical challenges, in particular reflection and shielding of the radar beam by mountains. A review of the challenges and sources of error, and the data processing techniques developed to mitigate them, e.g. terrain-aware algorithms and overlapping coverage, are presented in Germann et al. (2022). A reflectivity cap corresponding to a rainfall intensity of 118 mm h^{-1} is applied to prevent hail-induced overestimation (Liernur, 2023). Despite the inherent challenges, the radar system has been demonstrated to provide accurate and reliable rainfall estimates.

Although radar data are available from 2005, major upgrades were implemented in subsequent years, including the introduction of dual-polarisation (2012) and the installation of additional radars (2014 and 2016), which substantially enhanced rainfall estimation in the inner-Alpine regions (Germann et al., 2022). Given the homogeneity requirements of extreme value approaches, we restrict the analysis to 2016–2024.

2.2 Rain gauge network

Quality-checked measurements at 10-min resolution and 0.01 mm precision are obtained from 60 automatic rain gauges (Fig. 1), primarily Ott Pluvio2 weighing gauges, which are heated but unshielded from wind, as well as some tipping bucket Lambrecht gauges. The measurements undergo extensive internal quality control by MeteoSwiss (Musa et al., 2023). Gauges were required to contain at least 30 years of data (mean: 42.2 years) and be fully operational for the 9-year period covered by the radar. The network provides broad spatial coverage across flat, hilly, and mountainous terrain.

3 Methodology

3.1 Overview and study design

Extreme precipitation return levels are estimated using the non-asymptotic Simplified Metastatistical Extreme Value (SMEV) framework (Marra et al., 2019). Unlike traditional extreme value theory methods, which are based on maximum values of asymptotically large blocks (generally annual maxima) or exceedances over an asymptotically high threshold (Peaks-over-threshold), the SMEV estimates the distribution of extremes by assuming they are drawn from a finite sample of independent ordinary events. The statistical distribution used to model the tail of these ordinary events is derived from physical arguments (Wilson & Toumi, 2005). By using a significantly larger sample, rather than a limited set of extremes, the SMEV also allows one to describe heavy rainfall events not necessarily belonging to the category of extremes, and reduces parameter uncertainty

https://doi.org/10.5194/egusphere-2026-1800
Preprint. Discussion started: 18 May 2026

and allows for robust estimation of return levels from relatively short or error-prone records, making it particularly suitable for radar datasets (Dallan et al., 2024; Lengfeld & Marra, 2024; Marra et al., 2018, 2022).

The method's performance has been demonstrated across diverse climatic regimes, validating its underlying assumptions and capacity to reliably reproduce extreme precipitation frequencies (e.g. Marra et al., 2019; Miniussi & Marra, 2021; Rosin et al., 2024). Open-source code is available from Marra (2024). We adopt here the recent areal extension of the SMEV (Rosin et al., 2024), which enables estimation of extreme precipitation statistics across multiple spatial scales in addition to temporal aggregations.

3.2 Seasonal focus

The analysis is restricted to summer months (June-August), to ensure climatological consistency and optimal data quality. Precipitation extremes in Switzerland exhibit significant seasonality, strongly dependent on event duration and geographical location (Panziera et al., 2018). Winter extremes are typically synoptic, whereas summer extremes are predominantly convective up to daily timescales and spatial scales of order 100 km, though multi-day, large-scale extremes are often driven by synoptic-scale frontal systems. Restricting analyses to the relevant season is common in strongly seasonal climates, and many other studies have adopted a seasonal approach when analysing Swiss rainfall extremes (e.g. Fukutome et al., 2015; Haruna et al., 2023; Molnar & Burlando, 2008). The SMEV does not explicitly account for the seasonal nature of ordinary rainfall events (Falkensteiner et al., 2023); restricting the analysis to summer-only data satisfies the assumption that the ordinary events are independent and approximately identically distributed within the analysed sample (Marra et al., 2026).

From a data-quality perspective, radar performance in Switzerland is highest during summer in terms of distinguishing wet vs. dry periods, identifying extremes, and reducing overall bias relative to gauges (Barton et al., 2020), though summer data also exhibit the largest scatter, reflecting the highly localised nature of convective precipitation. Other seasons also introduce significant snowfall-related uncertainties, including radar reflectivity–snowfall conversion errors and wind-induced undercatch in gauges (Kochendorfer et al., 2017; Saltikoff et al., 2015), whereas summer precipitation is almost exclusively rainfall. Future studies could extend this analysis to other seasons.

3.3 Radar preprocessing and quality control

The radar-derived QPE data are extensively pre-processed by MeteoSwiss. We apply two further quality-control procedures to address known systematic biases and artefacts. First, comparisons of the radar QPE to rain gauge observations indicate an annual mean bias typically around zero. However, a seasonal bias pattern is present, characterised by overestimation in summer and underestimation in winter (Keller, 2013). We apply a multiplicative mean-field bias adjustment by scaling the QPE data by a factor of 0.87, derived from a radar–gauge comparison for the summer season.

Second, the radar QPE can be affected by hail contamination, causing overestimated radar rainfall measurements, even with the reflectivity cap applied (Cremonini et al., 2023). Radar–gauge studies have attributed overestimation of extremes to hail-related effects (Goudenhoofdt et al., 2017). To mitigate this, timesteps with a high likelihood of hail (>90%) are removed,

https://doi.org/10.5194/egusphere-2026-1800
Preprint. Discussion started: 18 May 2026

using the MeteoSwiss Probability of hail product, which provides radar-based estimates of the likelihood (0–100%) of hail reaching the ground at the same 1 km² and 5 min resolution as the QPE data (Nisi et al., 2016). This filtering reduces the possibility of including hail-induced artefacts. Although the cap alone already reduces the most extreme hail-induced artefacts at individual timesteps, relying solely on this threshold could still 'pollute' the statistics when applying extreme value methods. Although SMEV is less sensitive to such outliers than other approaches (Marra et al., 2018), the explicit removal of high-POH timesteps represents a more robust strategy for limiting hail-induced biases.

3.4 Event definition and sampling procedure

The areal-scale SMEV framework is based on the methodology of Rosin et al. (2024). Following Marra et al. (2020), ordinary events are based on storms, that is, independent meteorological objects identified as consecutive wet periods (intensity above 0.1 mm h^{-1}) separated by a continuous dry period of at least 24 h. This separation period balances maintaining statistical independence among storms with avoiding artificially splitting a single system by brief dry intervals.

Within each storm, one ordinary event is extracted for each duration-area combination (see below), defined as the maximum space-time averaged precipitation intensity. We consider durations of 30 minutes, 1, 3, 12 and 24 h, and areas of 1 (i.e. the radar pixel), 10, 50, 100 and 500 km², spanning short-duration rainfall events relevant to small, fast-responding catchments prone to flash flooding, as well as longer-duration forcings relevant to medium-sized basins (von Matt et al., 2025). The number of ordinary events is consistent across durations, meaning their distributions can be analysed across scales and linked to the underlying meteorological systems (Marra et al., 2020).

For spatial scales larger than 1 km², areas are represented using elliptical shapes centred on each radar pixel. For each event and for every duration–area combination, the ellipses are optimised with respect to both aspect ratio and orientation angle, ensuring that each extracted ordinary event represents the highest rain intensity for that specific scale. Further methodological details are provided in Rosin et al. (2024).

3.5 SMEV framework

The resulting ordinary events are used to estimate return levels within the SMEV framework. To isolate the distribution tail, parameter estimation is done via left-censoring, i.e., the lowest 90% of events are treated as non-exceedances of a proper threshold. This allows us to tailor the statistical model to the underlying physics-based assumptions (Wilson & Toumi, 2005). The 90% threshold was selected via a sensitivity analysis of the rain-gauge data (used due to the longer record length), to assess the null hypothesis of Weibull-tail behaviour (code available in Marra, 2022). This threshold has already been used in several studies focusing on the alpine region (e.g., Dallan et al., 2024).

The upper tail of the ordinary event distribution is modelled using a two-parameter Weibull distribution, following theoretical reasoning (Wilson & Toumi, 2005) and empirical evidence (Marra et al., 2023). The distribution is expressed as

$$\boldsymbol{F_{SMEV}(x) = [1 - e^{-\left(x/\lambda\right)^{\kappa}}]^{n}}, \quad (1)$$

https://doi.org/10.5194/egusphere-2026-1800
Preprint. Discussion started: 18 May 2026

where λ and κ are the scale and shape parameters of the Weibull distribution respectively, and n is the average number of storms per year.

The scale and shape parameters are initially estimated independently at each pixel for all area-duration combinations using a least-squares regression in Weibull-transformed coordinates (Marani & Ignaccolo, 2015). To mitigate sampling noise and the variability inherent in the short 9-year record, the shape parameter is then smoothed spatially using a 15 × 15 km^2 moving window. This window size was selected via a sensitivity analysis to pool sufficient information without over-smoothing the spatial variations and boundaries inherent in the rainfall data (orographic gradients, ridge lines, rain-shadows etc). The scale parameter is then re-estimated for each pixel using the original ordinary-event samples conditional on the new shape value. Smoothing the shape is preferable to smoothing the ordinary events, as this may bias the distribution before fitting and distort high-quantile return levels. As shown in Figs. S1 and S2, smoothing the shape significantly reduces the estimation uncertainty without notably affecting the magnitude of the derived return levels.

Although more sophisticated regionalisation methods have been applied previously to Swiss precipitation data (Haruna et al., 2022; Le Gall et al., 2022), the moving-window approach provides a simple, continuous regularisation that improves stability while preserving physically meaningful spatial gradients and avoiding artificial discontinuities.

Return levels are calculated from the smoothed-shape and re-estimated scale parameters for return periods of 2, 5, 10, 20, 50 and 100 years for all spatial and temporal scales. The associated estimation uncertainty is quantified using block bootstrapping (100 iterations), in which entire hydrological years (September 1 to August 31) are resampled to preserve the data's temporal structure (see Overeem et al., 2008). For each bootstrap replicate, the model parameters are estimated (including smoothing of the shape and recalculation of the scale) and used to compute the corresponding return levels. Uncertainty is then estimated as the 5th–95th percentile range of these estimates.

Finally, the return levels across all duration–area combinations are used to construct IDAF relationships, which extend traditional intensity–duration–frequency (IDF) curves by incorporating the spatial component. IDAF curves describe how return-level precipitation intensity varies jointly with duration, area, and return period.

3.6 Areal reduction factors

Areal reduction factors (ARFs) quantify the decrease in extreme rainfall intensity with increasing spatial aggregation. In the fixed-area formulation, ARFs are defined as the ratio between areal-average precipitation and the corresponding point location with the same exceedance probability.

Following the modified Bell method (Bell, 1976) commonly used in design-rainfall studies (e.g. Lutz et al., 2024; Svensson & Jones, 2010), we define the ARF as:

$$\mathrm{ARF}(D,T,A) = \frac{I_{(D,T,A)}}{I_{(D,T,0)}} \quad (2)$$

where I is the return-level rainfall intensity for a specific area A (with A approaching zero for a point measurement), duration D and return period T.

https://doi.org/10.5194/egusphere-2026-1800
Preprint. Discussion started: 18 May 2026

In classical point-to-area applications $A_0 \to 0$ represents a gauge measurement. However, as the Swiss gauge network is not sufficiently dense to provide robust point-to-area scaling, ARFs are computed relative to the 1 km² radar pixel, consistent with gridded-data ARF studies where the smallest resolved spatial support is used as the reference scale (e.g. Lutz et al., 2024).

4 Results

This section presents the return level estimates across spatiotemporal scales. Section 4.1 validates the radar-derived return levels against rain-gauge estimates. Section 4.2 presents the spatial patterns of return levels across Switzerland. Finally, Section 4.3 presents the derived IDAF curves and corresponding ARFs to investigate how extremes vary jointly with duration and area for different regions.

4.1 Validation against rain gauge derived return levels

Radar QPE estimates are subject to multiple sources of uncertainty, especially in complex terrain, which can affect the reliability of the derived return levels, despite the application of quality control procedures. To assess the reliability of the radar-based SMEV estimates, we therefore compare them against independent return level estimates calculated from gauge data. SMEV-based return levels are computed for all 60 gauges, and the corresponding radar-derived return levels extracted from the 1 km² radar pixel containing the gauge. As the gauge network is not sufficiently dense to support a robust evaluation at larger areal aggregations, the validation is restricted to the pixel scale. Unlike blended products such as CombiPrecip, the radar QPE used here is not adjusted using gauge data. The validation is therefore fully independent.

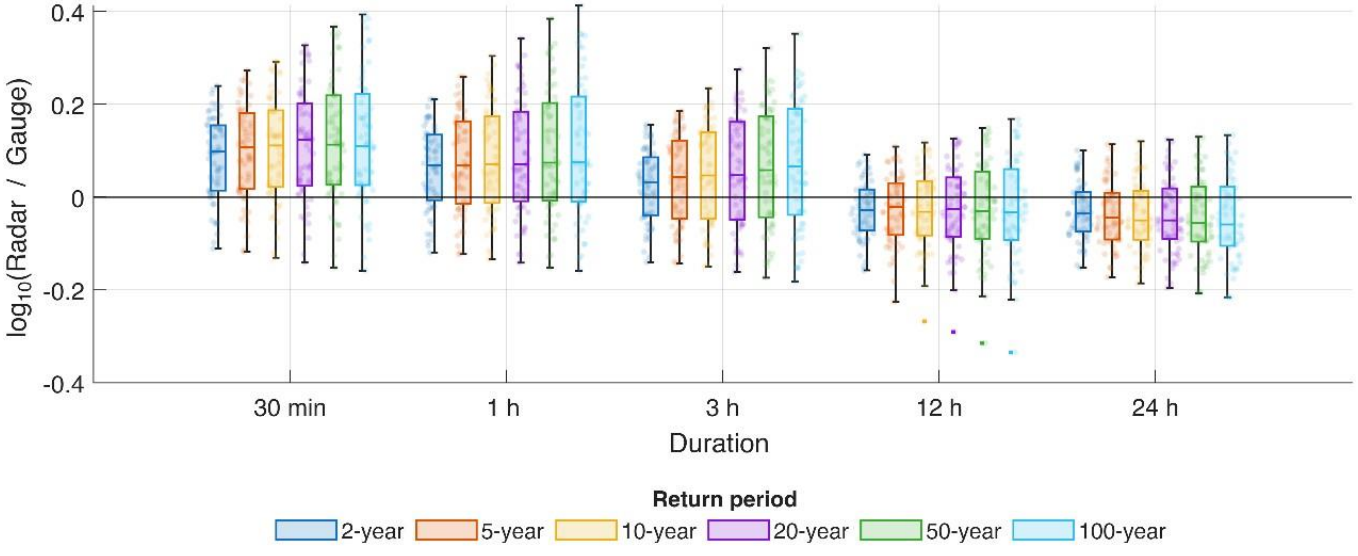

Figure 2. Bias between the radar- (1 km2 pixel scale) and gauge-derived return levels for return periods of 2, 5, 10, 20, 50 and 100 years and durations of 30 min, 1, 3, 6, 12 and 24 h.

https://doi.org/10.5194/egusphere-2026-1800
Preprint. Discussion started: 18 May 2026

Figure 2 summarises the bias for all 60 gauge-radar pairs across durations (30 min to 24 h) and return periods (2 to 100 years). Bias is expressed as $log_{10}(\frac{\text{Radar}}{\text{Gauge}})$, where 0 denotes perfect agreement. Each point represents a radar-gauge pair.

Overall, the radar and gauge derived estimates are broadly consistent, with 2-year bias values ranging from 0.1 at 30 min (overestimation of 26%) to -0.03 for 24 h (7% underestimation). A systematic duration dependence is evident, with radar generally exceeding gauge estimates for short durations (≤3 h) and underestimating at longer durations (12–24 h). Agreement improves with duration, evidenced by the decreasing inter-quantile range and spread. As expected, the interquartile range is higher for larger return periods due to the higher uncertainty, although the mean bias remains roughly constant. When gauge-based return levels are recomputed using only the 2016-2024 subset (not shown), the spread increases relative to the full record (consistent with higher sampling uncertainty from shorter records), but the overall bias pattern is preserved.

These findings are consistent with Haruna et al. (2024), who estimated the relative bias of seasonal 20-year return levels over Switzerland from 17 years of CombiPrecip reanalysis data, likewise observing short duration radar overestimation in summer and decreasing biases for longer durations, despite the use of a gauge-adjusted product. Figure 3 presents the radar-gauge bias spatial structure. Radar overestimation is most evident over the Jura and Central Alps, whereas underestimation is more prominent over the Plateau, Pre-Alps, and Southern Alps, with the magnitude and sign varying with duration. The spatial pattern is similar to that reported by Wolfensberger et al. (2021). The tendency toward radar overestimation at short durations contrasts with many previous studies that report systematic radar underestimation of point-scale extremes relative to gauges, largely attributed to sampling-volume differences and radar-specific limitations such as attenuation, range-dependent errors, and receiver saturation (e.g., Goudenhoofdt et al., 2017; Lengfeld & Marra, 2024; Overeem et al., 2009; Peleg et al., 2018; Post & Krajewski, 2023). At high spatial and temporal resolutions (e.g. 1 km, 5 min), wind effects and vertical variability in

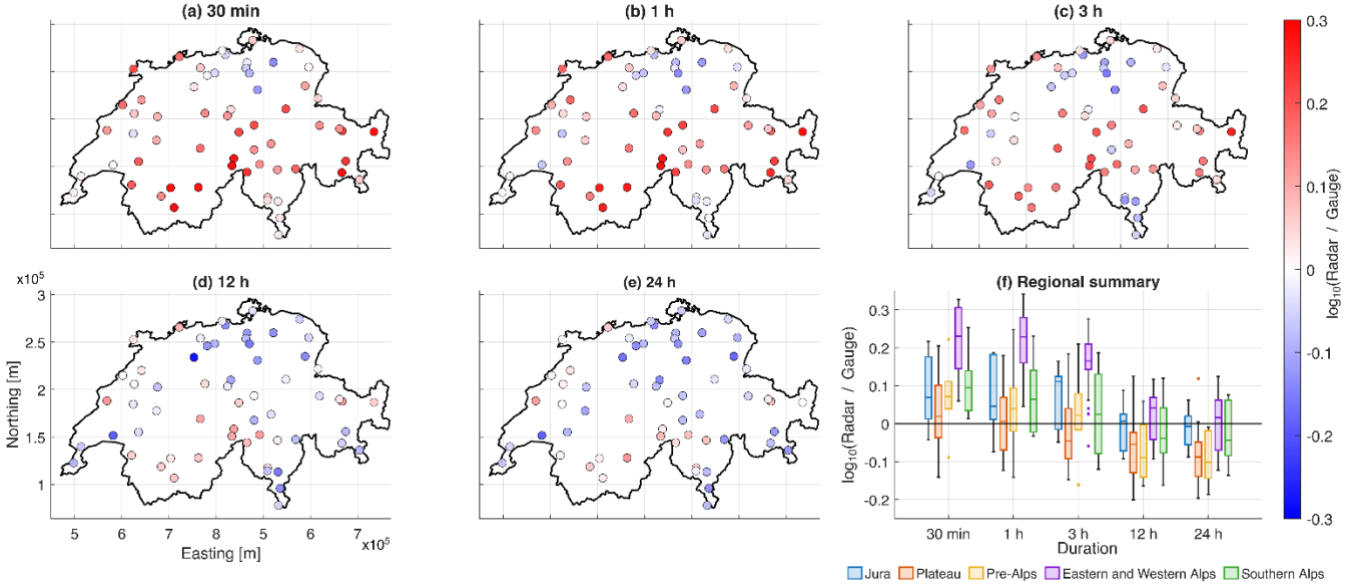

Figure 3. Bias between the radar- (1 km2 pixel scale) and gauge-derived 20-year return levels. Maps (a-e) show the radar-gauge bias at each gauge location. Boxplots (f) summarise the same bias by geographic region.

https://doi.org/10.5194/egusphere-2026-1800
Preprint. Discussion started: 18 May 2026

precipitation structure may cause additional biases (Dai & Han, 2014; Vasiloff et al., 2009). Radar-gauge agreement typically improves with increasing duration, as sharp, short-lived rainfall peaks are smoothed through temporal accumulation (Bayabil et al., 2019; Schleiss et al., 2020).

Several mechanisms can plausibly contribute to the observed overestimation here. Radar may capture small sharp peaks that the gauges miss when the gauge is offset from the highest intensity rainfall within the 1 km² pixel. Additionally, though gauge data are often used as ground truth, they also contain errors and biases, most significantly wind-induced undercatch (typically 5–10% for ordinary events but exceeding 30% during extremes) which disproportionately affects short durations (Pollock et al., 2018; Sieck et al., 2007). More specific to the regional context, the Swiss radar QPE system is extensively configured and quality-controlled for local conditions (complex topography and prevalent precipitation regimes), and this tuning may yield residual error characteristics that differ from those of other products or regions. Finally, the summer multiplicative bias adjustment (factor 0.87; Section 2.1) likely affects the radar-gauge agreement. Increasing the factor could reduce short-duration bias but would likely increase underestimation at longer durations.

It should also be noted that exact agreement is not expected between the gauge and radar estimates, even with perfect measurements, as gauges capture point-scale measurements, whereas radar QPE represents a spatially averaged value over a 1 km² pixel and therefore contains small-scale variability (Gires et al., 2014). This 'representativeness gap' is most pronounced at very short accumulation times (under 5 min according to Villarini et al., 2008) and longer return periods (Peleg et al., 2018).

4.2 Spatial maps of return levels

Figure 4 presents the estimated 20-year radar-derived return levels for 1, 10 and 100 km^2 areas, and for durations of 30 min, 3 and 24 h. Additional scales are shown in Fig. S3. Across Switzerland, the spatial structure of extremes depends strongly on both temporal and spatial aggregation, with topographic gradients exerting a major role. For short durations and small areas (30 min-1 h, 1-10 km²) extremes are more localised, with the highest rainfall intensities occurring over the Southern Alps, and secondary maxima along the transition zones between the plains and foothills of the Alpine barrier and the Jura mountains. In contrast, the inner valleys of the Eastern and Western Alps and the Plateau show significantly lower values. As duration increases, the Alpine/Jura enhancement weakens, whereas the Southern Alps hotspot persists across all temporal scales. The same duration-dependent pattern was found by Haruna et al. (2023) in their station-based IDF analyses across Switzerland for 1 and 24-h 100-year return levels.

The spatial pattern also resembles the climatology of warm season 1 km^2 extremes reported by Panziera et al. (2016, 2018), using CombiPrecip data (MeteoSwiss, 2018a; Sideris et al., 2014). They attribute the observed distribution to instability along the alpine slopes which can be easily released through orographic forcing, a mechanism absent over the Swiss Plateau. Conversely, at higher altitudes near the alpine crest convection is inhibited due to less moisture availability. For all scales, few radar artefacts are visible despite the complex mountainous terrain. This can be attributed partly to the overlapping coverage provided by a network of five radars.

https://doi.org/10.5194/egusphere-2026-1800
Preprint. Discussion started: 18 May 2026

Increasing the areal scale substantially alters both the magnitude and spatial structure of extremes. For all durations, local peaks become progressively smoothed, with fewer, broader zones of higher intensity. The region of enhanced rainfall following the west to east band of topography along the Alps disappears, while the Jura mountains maintain moderately elevated return levels. Again, the Southern Alps remain the dominant centre of high intensity, with increasing prominence for longer durations. These spatial patterns are mirrored by the fitted Weibull parameters (Figs. S4 and S5). The scale parameter, which primarily controls return-level magnitude, decreases systematically with increasing spatial and temporal aggregation. The shape parameter governs tail behaviour, with a smaller shape implying a slower-decaying (heavier) tail and a greater tendency for large extremes relative to the ordinary events. The shape increases generally with both duration and area. For small area–duration combinations the Southern Alps and Central Alps exhibit high shape values, whereas at long durations the Southern Alps combine a high scale with a lower shape, indicating comparatively heavier-tailed behaviour.

Figure 5 illustrates how these spatial patterns evolve with return period for one representative space-time combination (30 min; 50 km²). The overall spatial distribution of maxima and minima remains generally constant as return period increases. However, regional contrasts intensify, and some structural changes emerge, including a narrowing of the Southern Alps

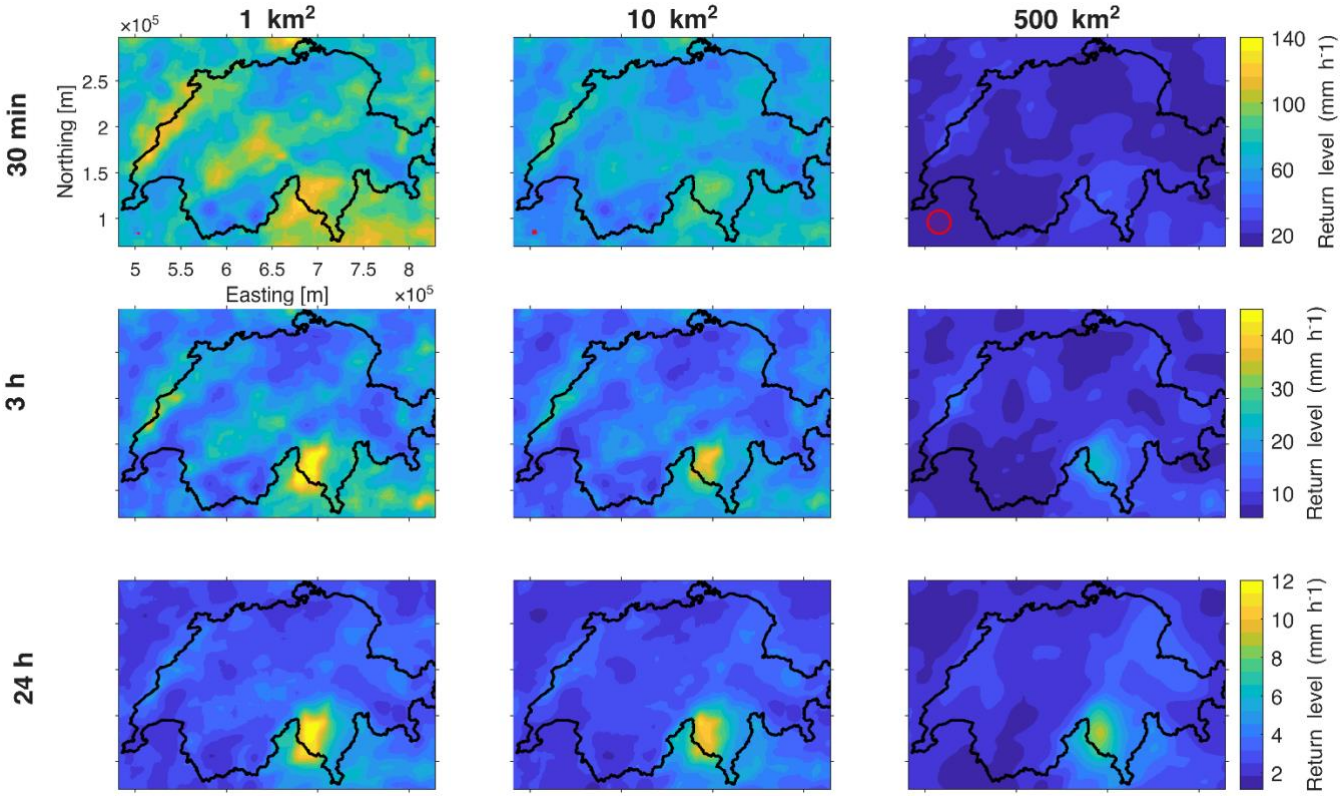

Figure 4. Spatial distribution of 20-year rainfall return levels across durations and aggregation areas. Return levels are shown in mm h⁻¹ for durations of 30 min, 3, and 24 h and for areas of 1, 10, and 100 km². Red circles in the top row indicate the equivalent spatial extent of each areal scale.

https://doi.org/10.5194/egusphere-2026-1800
Preprint. Discussion started: 18 May 2026

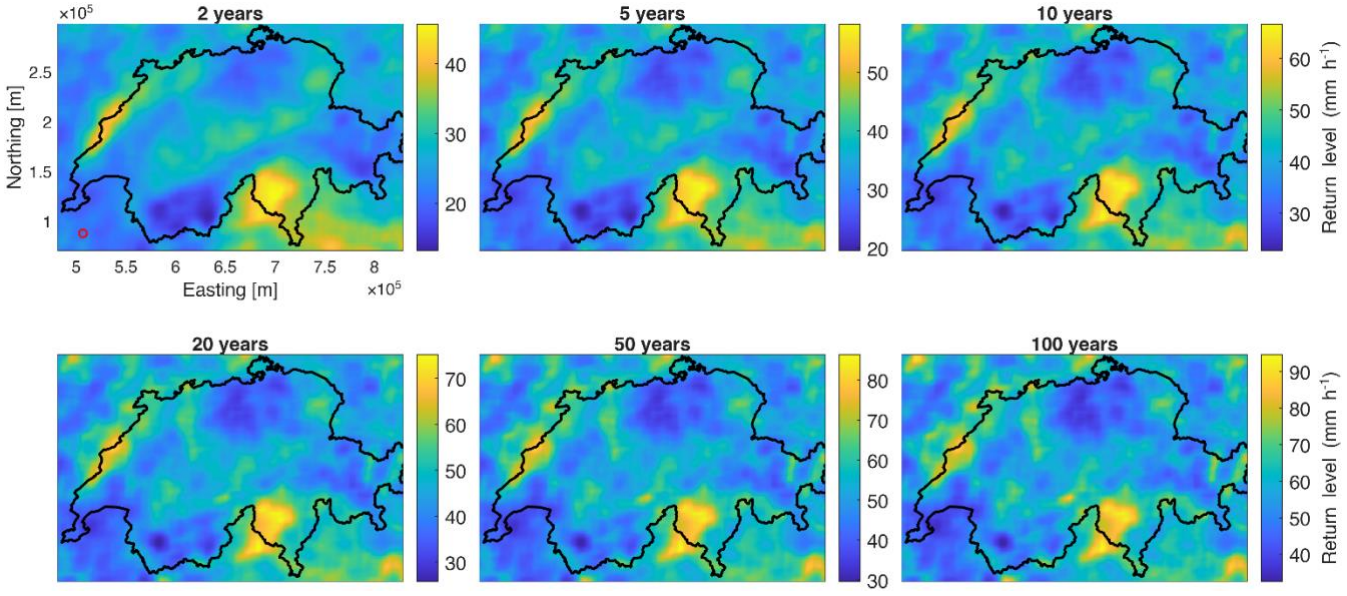

Figure 5. Spatial distribution of 30-min rainfall return levels (mm h⁻¹) for a 50 km² aggregation area and return periods from 2 to 100 years. Colour scales differ between panels to emphasise spatial structure at each return period. Red circle (first panel) indicates the equivalent spatial extent of the 50 km² aggregation area.

maximum and reduced distinctness of the elevated return levels along the Alpine ridge. Similar behaviour is observed across other duration–area combinations.

4.3 IDAF curves

To summarise the joint dependence of extremes on duration and area, we construct IDAF relationships for six distinct geographic regions. For every duration–area combination, regional return levels are computed as the spatial average of the estimated return levels within a 10 × 10 km^2 region-specific box (Fig. 1), in order to suppress fine-scale sampling noise and radar artefacts. Uncertainty is shown as 90% confidence intervals derived from 100 bootstrap repetitions, computed by first calculating the spatial mean return level within each box for every bootstrap realisation and then taking the corresponding percentile range. Figure 6 presents 20-year IDAF curves for each region (additional return periods and fitted parameters are shown in Fig. S6). Figure 7 presents the same curves, organised by duration, and includes the R^2 of the linear regression between the log-transformed intensity and duration. Figure 8 presents the corresponding ARF values.

https://doi.org/10.5194/egusphere-2026-1800
Preprint. Discussion started: 18 May 2026

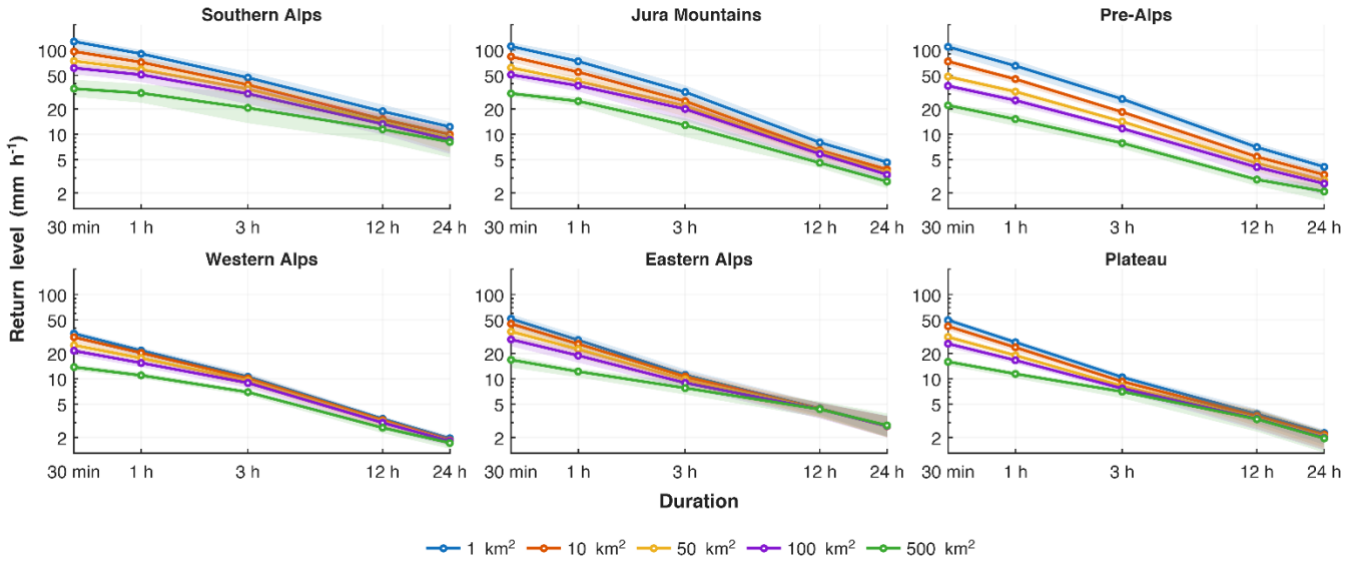

Figure 6. IDAF curves estimated for 20-year return periods for the six analysis regions. Shaded areas represent the 90% confidence intervals from 100 bootstrap samples. The locations of the regional analysis boxes are shown in Fig. 1.

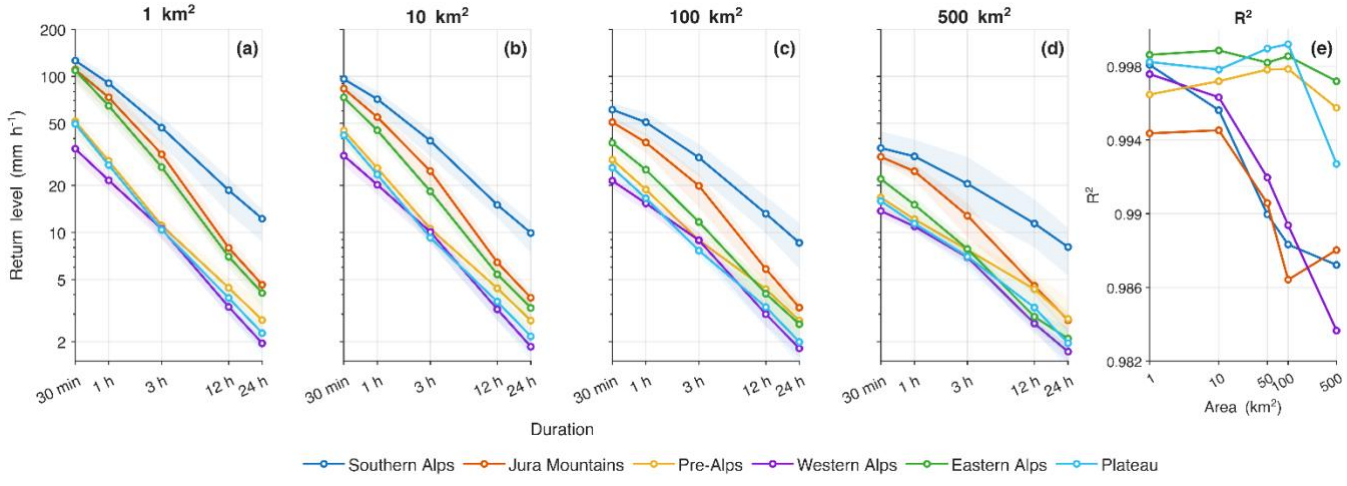

Figure 7. (a – d) Twenty-year rainfall return levels as a function of duration for increasing aggregation areas. Shaded areas represent the 90% confidence interval from 100 bootstrap samples. The locations of the analysis sites are displayed in Fig. 1. (e) Coefficient of determination (R^2) from the linear regression between log-transformed return level and log-transformed duration, as a function of area. Analysis-box locations shown in Fig. 1.

Return levels decrease significantly with both increasing spatial and temporal scale, with clear regional contrasts. The highest return levels occur over the Southern Alps, Jura, and Pre-Alps, as expected. The 90% uncertainty bounds are overall narrow, due to the spatial smoothing of the Weibull shape parameter, which increases the effective sample size and reduces sampling noise. In line with this interpretation, IDAF curves derived without shape smoothing exhibit substantially larger uncertainty (see Fig. S2). Properties of the derived IDAF curves and parameters are discussed further in Section 6.

https://doi.org/10.5194/egusphere-2026-1800
Preprint. Discussion started: 18 May 2026

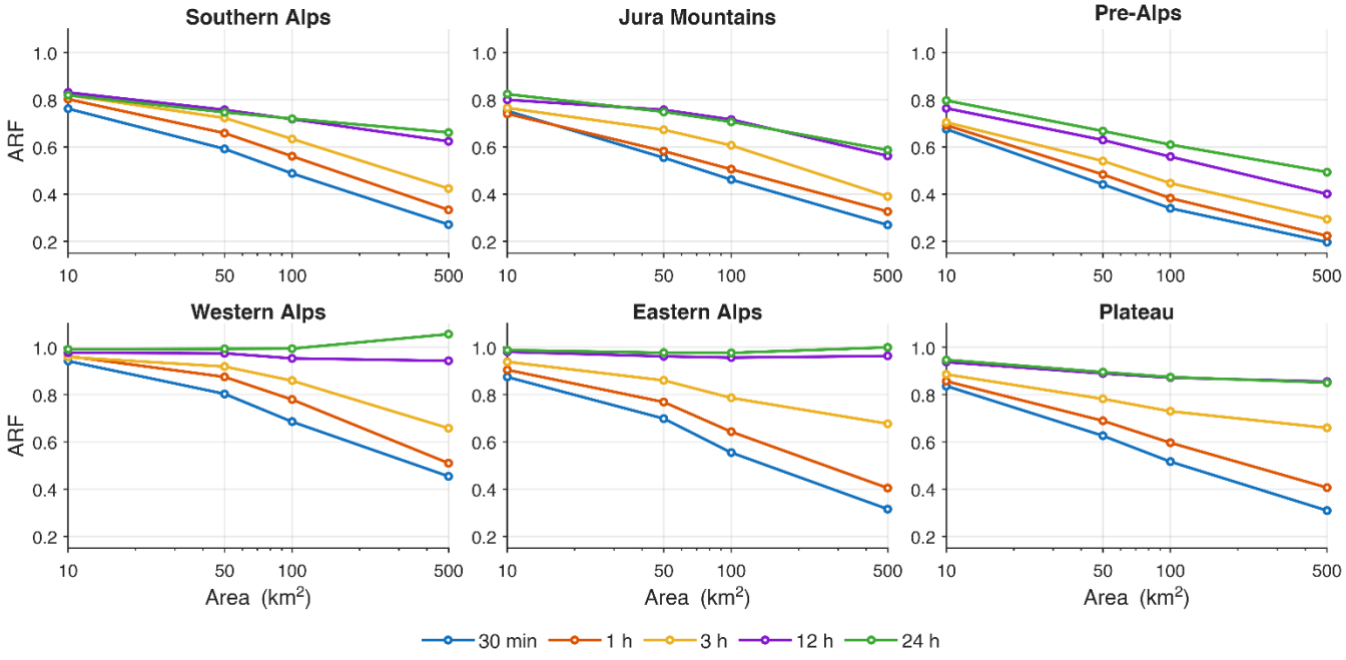

Figure 8. ARFs estimated for 20-year return periods as a function of aggregation area for the six analysis regions. Regional analysis-box locations are shown in Fig. 1.

5 Extreme precipitation severity and associated hydrological hazards

A practical utility of the derived IDAF relations lies in their ability to characterise the severity of a storm across different hydrologically relevant spatiotemporal scales, and relate this directly to hydrological hazard, unlike traditional point-based intensity–duration estimates, which provide limited insight into the spatial footprint of rainfall. This methodology effectively constructs severity diagrams, a tool used to evaluate the rarity and impact of a specific storm event across multiple spatial and temporal scales (Ramos et al., 2005).

We apply this approach to three recent high-impact events in Switzerland (Fig. 9) that represent a spectrum of hydrological responses:

(i) 21 June 2024 - *Mesolcina Valley (Southern Alps):* flash flooding, debris flows
(ii) 11 June 2018 - *Lausanne (Western Plateau):* urban flooding
(iii) 15 July 2021 - *Central Alps and Plateau*: prolonged river and lake flooding

All events produced destructive flooding and infrastructure damage, with fatalities reported in the first case. For each event, the associated precipitation event is identified and the corresponding return period computed for every duration–area combination using the estimated SMEV-based IDAF relations. This enables a direct evaluation of the event severity across spatiotemporal scales and identifies the scales most consistent with the observed hydrological response. Owing to space constraints, only selected areas and durations are shown.

https://doi.org/10.5194/egusphere-2026-1800
Preprint. Discussion started: 18 May 2026

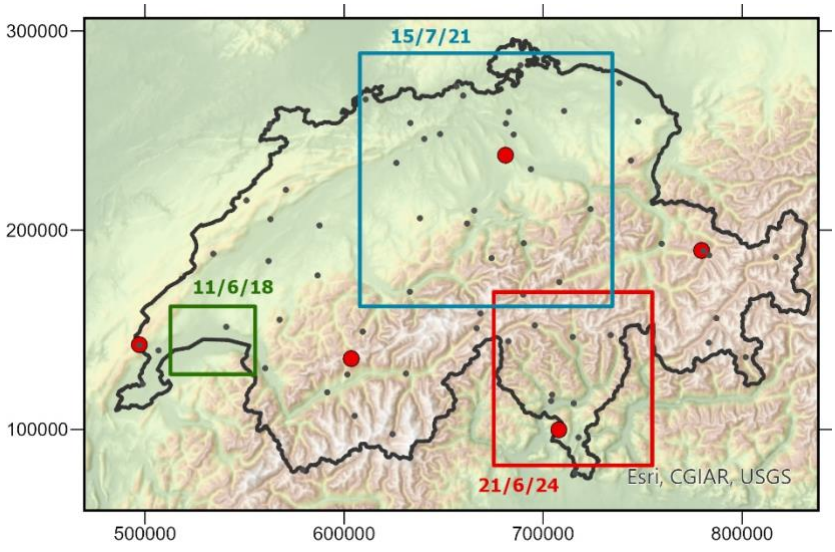

Figure 9. Locations of the three extreme hydrological events. Coloured rectangles indicate the analysis domains for each event. Red circles mark the locations of the five radar stations, and black circles indicate rain gauge locations. The corresponding multiscale severity diagrams for these events are shown in Figs. 10–12. Basemap sources: Esri, CGIAR, USGS | Powered by Esri.

(i) 21 June 2024

In June 2024 an advancing cold front from a France–Germany low overran a warm, moisture-rich subtropical air mass south of the Alps, triggering intense, short-duration rainfall along the south-Alpine slopes, especially the Mesolcina valley and Valais. The Grono gauge measured 124 mm in 24 h, including 63 mm in one hour (MeteoSwiss, 2024). Combined with snowmelt, this generated substantial runoff, causing extensive damage and several casualties.

IDAF-derived multi-scale severity diagrams depicting the calculated return periods for this event are presented in Fig. 10, while Fig. 9 displays the geographical extent of the analysed area. The return periods indicate strong spatial and temporal variability, with the most extreme, spatially extensive rainfall occurring at short durations over large areas (30 min, 100-500 km^2) and at intermediate durations over small areas (12 h, 1-10 km^2), where return periods exceed 100 years. Conversely, 24 h accumulations remained comparatively modest across all area scales.

Hydrologically, these patterns imply the highest hazard for small to medium-sized catchments with sub-hourly to multi-hour response times, favouring flash flooding and debris flows developing within a few hours, consistent with the observed impacts. In the steep Mesolcina catchments, intense multi-hour rainfall rapidly exceeded infiltration and channel capacity, producing sharp rises in streamflow, runoff and debris flows. However, the rainfall lacked the duration to drive major flooding in larger river basins, which typically require more sustained accumulation to exceed their larger storage thresholds.

https://doi.org/10.5194/egusphere-2026-1800
Preprint. Discussion started: 18 May 2026

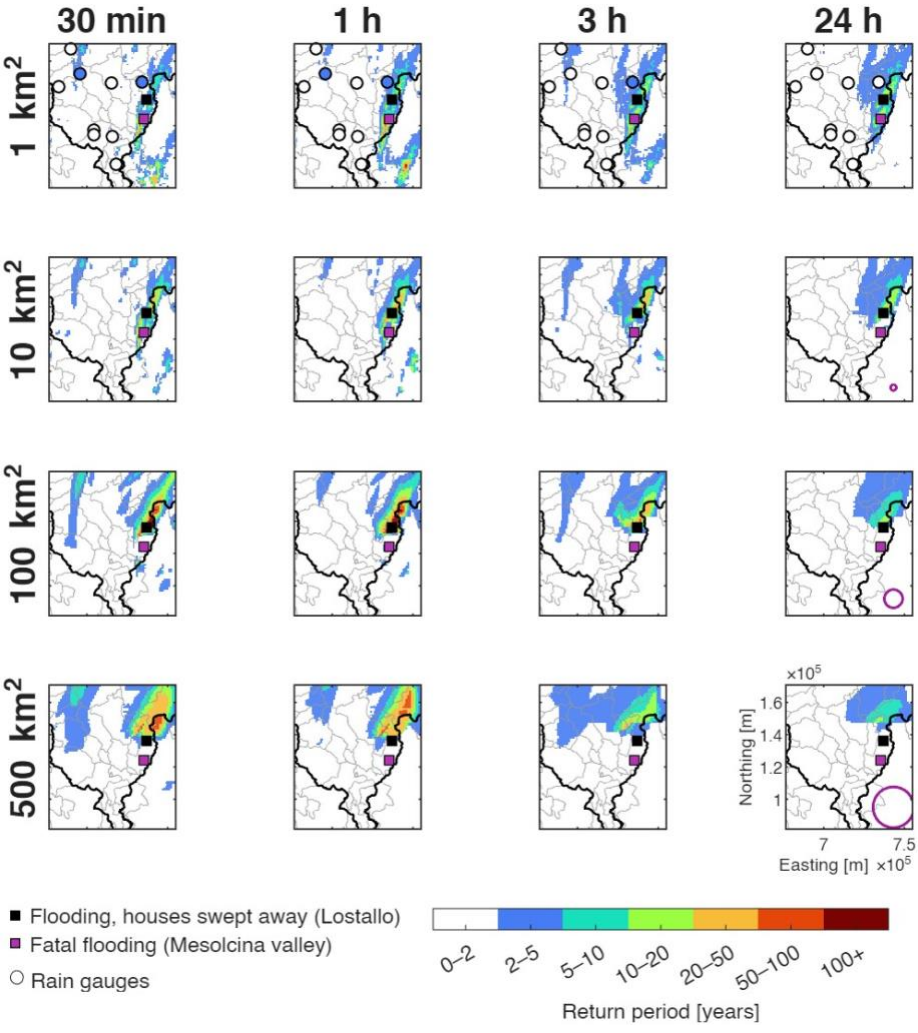

Figure 10. Radar-derived rainfall return periods for the 21 June 2024 event across multiple spatiotemporal scales. Columns show accumulation durations of 30 min, 1 h, 3 h, and 24 h, while rows correspond to aggregation areas of 1, 10, 100, and 500 km². Catchments boundaries are shown in grey. Circles (top row) indicate rain gauge locations, coloured by the corresponding gauge-derived return periods. Purple circles (rightmost column) indicate the equivalent spatial extent of each areal scale.

A significant discrepancy exists between the gauge and radar-derived return periods. Most gauges, located outside of the storm core, recorded return periods under 5 years for all temporal scales, whereas radar captured the narrow but intense rainfall band, enabling a more realistic estimation of the event's scale-dependent extremes and spatial structure.

(ii) 11 June 2018

On 11 June 2018, a severe convective storm developed over the Lausanne urban area, producing the most intense short-duration rainfall event recorded in Switzerland. A downtown gauge measured a national 10-minute record (40.9 mm), with extreme 5 min bursts (23.7 and 17.2 mm), and a steep spatial gradient (the Pully gauge 2.5 km away recorded 17.1 mm during the same

https://doi.org/10.5194/egusphere-2026-1800
Preprint. Discussion started: 18 May 2026

hour). Gauge networks are rarely dense enough to ensure that at least one instrument is located sufficiently close to the rainfall maximum in deep convective storms. In this case, however, the gauge measurement is likely near representative of the true peak intensity (Gabella et al., 2018). The resulting urban flash flooding in the city centre caused significant infrastructure damage, particularly of the sewer network, costing CHF 27 million (Gabella et al., 2019; MeteoSwiss, 2018b).

The severity diagrams (Fig. 11) confirm that rainfall close to Lausanne was dominated by very short duration, small footprint rainfall. Return periods greater than 5 years occurred only for 30 min to 3 h durations and for small areas (1-10 km^2), with values decreasing rapidly with both temporal and areal aggregation. Though basin-scale return periods were relatively modest, local peak intensities rapidly overwhelmed the drainage network and produced severe pluvial flooding. This disparity between catchment-average and local rainfall emphasises the need for sub-kilometre, sub-hourly characterisation of rainfall extremes in urban flood-risk assessment and design.

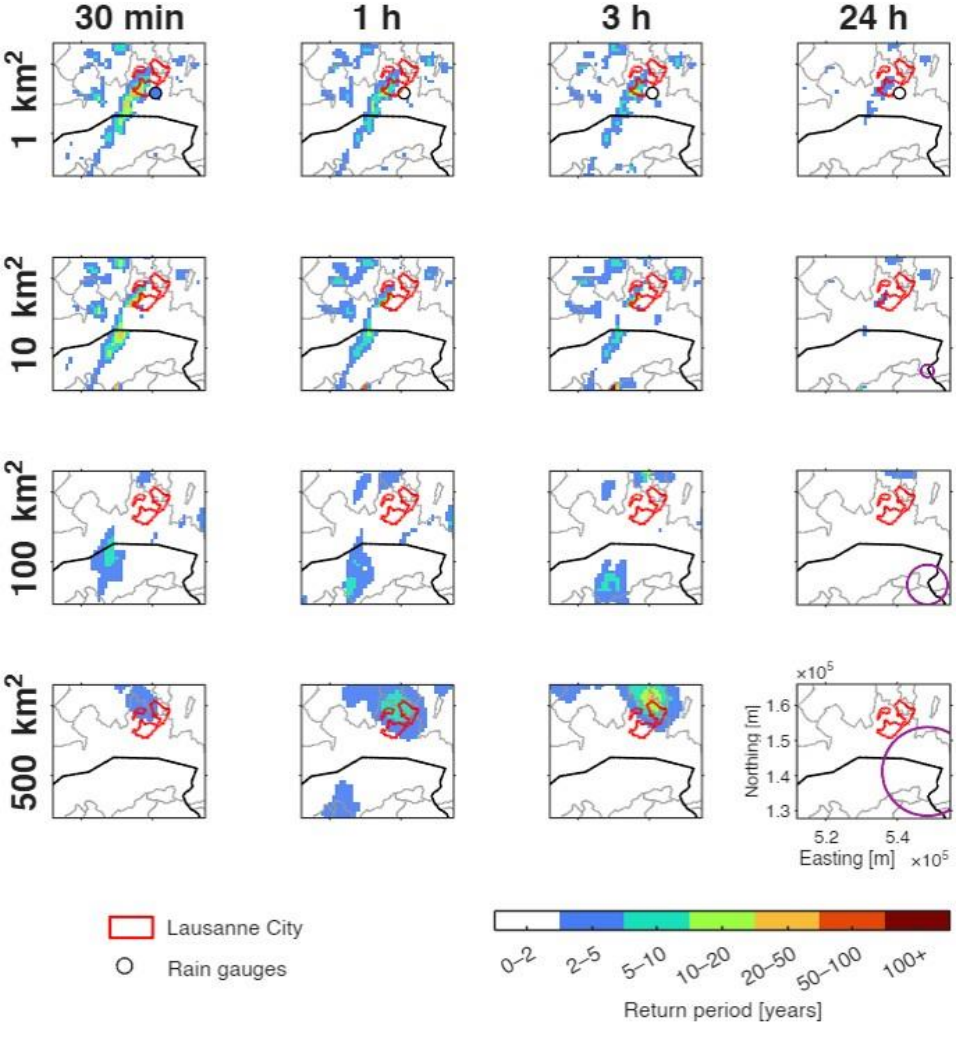

Figure 11. Same as Fig. 10, but for the 11 June 2018 event.

https://doi.org/10.5194/egusphere-2026-1800
Preprint. Discussion started: 18 May 2026

However, even at the smallest aggregation considered (1 km^2 and 30 min), the maximum radar-derived return period is only 33 years, in contrast with a return period exceeding 3000 years for the downtown gauge. This discrepancy partly reflects the scale mismatch between point measurements and areal radar estimates, where a radar pixel represents the mean areal rainfall over a 1 km² area, and therefore attenuates highly localised peaks that can occur over scales of only a few hundred metres (Peleg et al., 2018).

In addition, Gabella et al. (2018) assert that deviations from the assumed exponential drop size distribution (DSD) also led to a severe underestimation of the 1 km^2 radar QPE peak rainfall during the event, when using the standard operational Swiss-tuned Z–R relationship. Under this relationship, the instantaneous radar-derived rate near the core is measured at 124 mm h^{-1}, whereas adopting a maritime-tropical Z-R relation yields 265 mm h^{-1}, in closer agreement with the gauge. This highlights the challenges radar faces in capturing accurate quantitative estimation of rainfall amounts at the ground, particularly for short-lived, sub-kilometre tropical-like convective peaks in complex terrain.

(iii) 15 July 2021

In contrast to the convective bursts described above, July 2021 saw prolonged heavy rainfall driven by cool moist air masses rising from the Atlantic. Precipitation totals exceeded 100 mm across extensive areas, with 150 mm recorded along the northern Alpine slopes (FOEN, 2023). Hydrologically, the event was characterised less by sharp peaks and more by sustained high flows and persistently elevated lake levels. Lake Lucerne reached a record July level, while Lake Zurich remained critically high for nearly six days. Impacts included flooded basements and infrastructure, erosion, and landslides, with total damages reaching approximately CHF 60 million (FOEN, 2023).

The severity diagrams (Fig. 12) depict a rainfall structure consistent with these hydrological impacts. Short-duration accumulations (30 min - 3 h) exhibit uniformly low return periods (generally under 10 years, especially for small areas), whereas 12–24 h durations show large regions with high return periods, locally exceeding 50–100 years, reflecting the event's prolonged, large-scale nature. Despite the widespread extent, the gauge network largely missed the highest intensity rainfall, with only one gauge recording a return period above 50 years.

Overall, these cases demonstrate that hydrological hazard cannot be characterised by a single duration or point-scale intensity, with all three events displaying different but pronounced scale dependence. A single storm can yield rainfall with a return period of the order of 100 years at one duration–area combination and under five years at another. Moreover, excluding the Lausanne event, the most extreme rainfall was under-sampled or entirely missed by the gauge network, whereas radar-based IDAF analysis captured the spatial organisation and scale dependence of the extremes. Robust flood-hazard assessment, especially in complex terrain, should therefore involve multi-scale analysis of rainfall behaviour rather than reliance on storm totals alone.

https://doi.org/10.5194/egusphere-2026-1800
Preprint. Discussion started: 18 May 2026

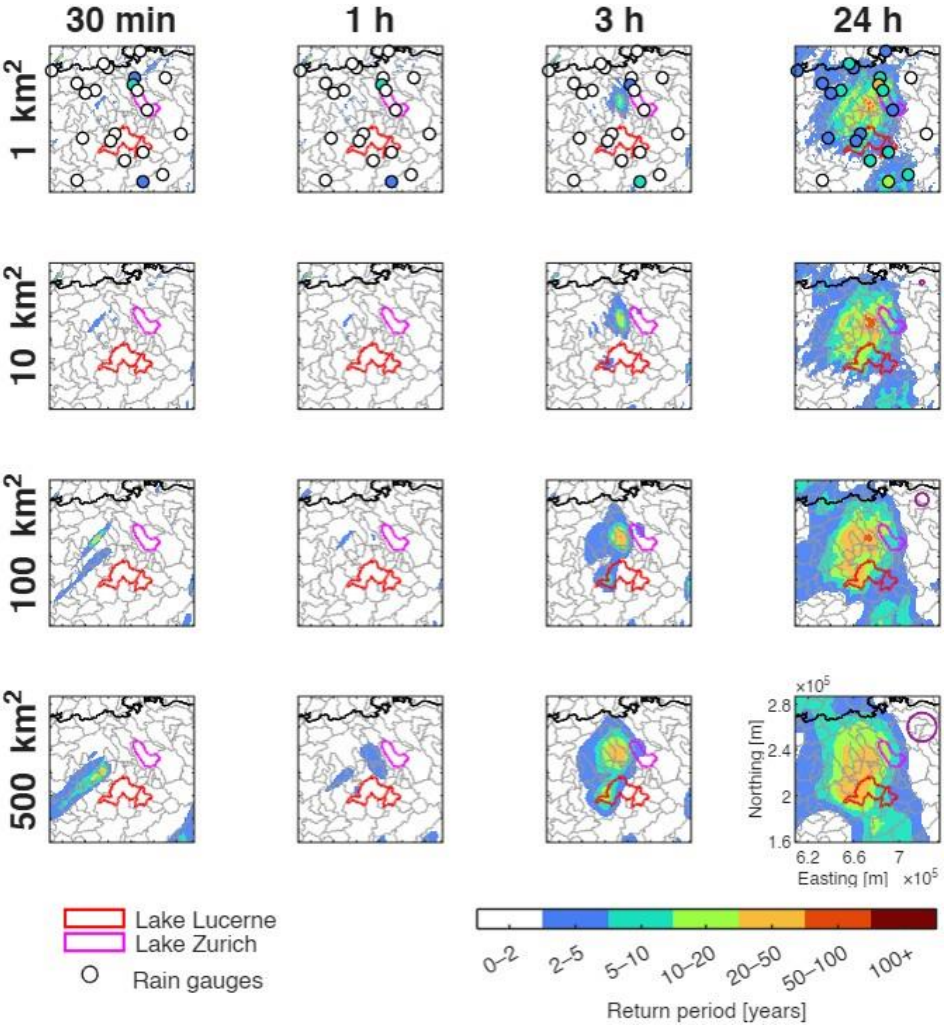

Figure 12. Same as Fig. 10, but for the 15 July 2021 event.

6 Discussion

6.1 Dependence of extreme precipitation on spatial and temporal scale

Rainfall extremes exhibit systematic scaling relationships with both duration and area, a phenomenon widely documented in hydrometeorological literature (Menabde et al., 1999). The IDAF relationships derived here provide a high-resolution framework for evaluating these dynamics across the complex topography of Switzerland.

The dependence of return levels on duration observed in Fig. 6 is consistent with previous multi-scale analyses (Haruna et al., 2024; Rosin et al., 2024). At short durations and small spatial extents, rainfall is localised, and a single rain cell can cover the entire analysed area - meaning the areal average is close to the cell peak. As aggregation area increases beyond the typical cell

https://doi.org/10.5194/egusphere-2026-1800
Preprint. Discussion started: 18 May 2026

size, spatial heterogeneity increases and lower intensity regions enter the domain, reducing the areal average. At longer durations, however, multiple rainfall cells may enter the accumulation window, leading to increasingly similar intensities across all area sizes. Notably, Rosin et al. (2024) found this behaviour consistent across coastal, desert, and mountainous regions, despite the substantial differences in geography and precipitation regimes.

The magnitude of this areal scaling varies markedly between regions across Switzerland. The Pre-Alps, Jura, and Southern Alps exhibit the smallest ARF values and the steepest intensity decline with spatial scale for all durations, physically consistent with the dominance of intense orographically forced convective storms. Spatial reduction is significantly stronger for convective events than stratiform (20–30% higher according to Eggert et al. (2015)). The Southern Alps experience the highest frequency of severe deep convective precipitation while the elevated terrain in the Pre-Alps and Jura also drives high convective activity (Feldmann et al., 2023).

Notably, in contrast to the near convergence of IDAF curves at long durations reported by Rosin et al. (2024), the Pre-Alps, Jura, and Southern Alps retain clear intensity distinctions between aggregation areas even for extended durations. This suggests that convective systems in complex terrain can maintain sharp spatial gradients and pronounced intermittency over prolonged periods. Convective precipitation typically exhibits lower advection velocities than stratiform precipitation (Eggert et al., 2015), and in mountainous environments this effect can be amplified by orographic anchoring. Interactions between mesoscale flow and topography can repeatedly trigger and sustain convection over the same windward slopes and valleys (Feldmann et al., 2023), favouring (quasi-)stationary convective cell trains.

Such organisation limits the spatial 'smearing' of rainfall that would otherwise occur with increasing duration, thereby preserving contrasts between aggregation areas. Importantly, the principal hazards in complex terrain are often associated not only with isolated severe convective cells, but additionally with these persistent, topographically modulated convective systems, which in aggregate can generate extreme rainfall totals and substantial impacts including flash floods, landslides, and debris flows (Panziera et al., 2015; Panziera & Germann, 2010).

Other regions display different behaviours. The Plateau exhibits strong areal reduction at short durations, but significant convergence by 12–24 h, consistent with a transition from localised convection at short durations to more spatially extensive precipitation associated with synoptic-scale flow at longer durations (Panziera et al., 2018). The Eastern and Western Alps exhibit the weakest areal reduction (highest ARFs) and near full convergence of IDAF curves at long durations, indicating reduced spatial variability and more homogeneous storm structures. These inner-Alpine valleys lie in pronounced rain shadows where incoming air masses are partially depleted on the outer slopes (Frei & Schär, 1998), short duration extremes are linked to local thermally and topographically triggered convection, whereas 12–24 h accumulations arise from synoptic-scale precipitation enhanced by orographic forcing (e.g. Panziera et al., 2018).

The Western Alps exhibit a 24 h ARF value exceeding 1. Empirical values of ARFs exceeding 1 have been already reported (Catchlove & Ball, 2003; Haruna et al., 2024) and are possible in locations with strong precipitation gradients. This suggests that rainfall intensity at the reference pixels is located on the shielded valley. As aggregation area increases, higher rainfall amounts from the adjacent, more exposed slopes enter the domain, leading to a higher areal average.

https://doi.org/10.5194/egusphere-2026-1800
Preprint. Discussion started: 18 May 2026

Across all regions, the observed spatiotemporal patterns are broadly consistent across return periods from 2 to 100 years, however the differences between area sizes become increasingly pronounced at higher return periods (Fig. S6). This aligns with findings that rarer events have a greater relative contribution of localised convective rainfall, reducing the ratio of areal to point rainfall (Allen & DeGaetano, 2005; Asquith & Famiglietti, 2000).

To further illustrate how topography and location modulate extremes in a scale-dependent manner, we analyse four transects of normalised return levels across the region and the associated SMEV shape parameter (Supplement S3; Figs. S6–S7). The transects further show that the influence of duration and aggregation area on rainfall extremes varies markedly between locations.

6.2 Simple versus multiscaling behaviour

The derived IDAF curves also enable an assessment of the scale invariance of extreme precipitation over areal scales. Under simple scaling, extreme rainfall intensity follows a power-law dependence on duration and area, implying approximately linear behaviour in log–log IDAF space with scale-invariant exponents. Multiscaling arises when the scaling exponent varies with scale, producing curvature or slope changes. Physically, simple scaling holds when extremes are governed by a dominant rainfall regime and storm structures remain self-similar under aggregation. Multiscaling occurs when rainfall aggregation spans heterogeneous processes or finite storm size becomes important (Panthou et al., 2014). Marra et al. (2026) demonstrated recently that process heterogeneity is an essential component of extreme sub-daily precipitation statistics in this area, with apparent heavy tails at intermediate sub-daily durations emerging from mixtures of convective and stratiform precipitation rather than from intrinsically heavy-tailed processes.

Simple scaling of rainfall extremes with duration is well validated at the point scale (Blanchet et al., 2016; Bougadis & Adamowski, 2006). At larger spatial scales evidence becomes more mixed. Several studies found simple-scaling formulations effective for durations up to 24 h and areas extending from the point scale to over 500 km^2 (Nhat et al., 2007; Panthou et al., 2014). Rosin et al. (2024) observed prominent simple scaling at the pixel scale but progressive weakening under spatial aggregation. Some frameworks utilise comprehensive multiscaling methods (e.g. De Michele et al., 2001), or more flexible 'middle ground' frameworks that relax strict space–time dynamic scaling (Giudicianni, 2026; Mélèse et al., 2018).

The IDAF relationships for Switzerland (Fig. 7) remain near linear in log–log space across all the analysed spatial scales. R^2 values from linear regression between the log-transformed 20-year intensity and duration exceed 0.98 for all area sizes, suggesting the extreme rainfall processes remain largely self-similar under aggregation, despite the physical complexity of summer convective processes. This is notable as summer Alpine precipitation is typically associated with high intermittency and convection, conditions often linked to multiscaling behaviour (Molnar & Burlando, 2008).

From an applied standpoint, this near-simple scaling behaviour is advantageous as it supports the parsimonious temporal downscaling of rainfall extremes across different area scales, e.g. estimating sub-daily extremes from daily data using power-law relationships (Bougadis & Adamowski, 2006; Yamoat et al., 2023).

https://doi.org/10.5194/egusphere-2026-1800
Preprint. Discussion started: 18 May 2026

7 Conclusions

Extreme precipitation in complex Alpine terrain exhibits strong spatial and temporal variability, posing substantial challenges for the estimation of statistically robust, design-relevant return levels. We address this challenge by combining a nine-year (2016–2024) radar-derived QPE archive with the areal Simplified Metastatistical Extreme Value (SMEV) framework to produce a high-resolution climatology of summer (June-August) extremes for Switzerland. Return levels are estimated for durations from 30 min to 24 h and areas from 1 to 500 km², over return periods up to 100 years. The resulting Intensity–Duration–Area–Frequency (IDAF) relationships provide a physically interpretable description of how extreme rainfall varies across space and time over complex terrain.

Despite the short record length, the SMEV approach with regionalised estimation of the shape parameter yields stable multiscale return level estimates. Validation against 60 long-term gauges demonstrates that the radar-derived return levels are regionally consistent and reliable, even in topographically complex regions with high sampling variability.

Rainfall extremes exhibit a pronounced dependence on spatial and temporal scale. Short duration (≤3 h), small areas (≤50 km²) extremes are more localised and primarily associated with intense convective storms, with significant maxima over the Southern Alps and along the transition zones between the plains and foothills of the Alpine barrier and the Jura mountains. Persistent minima are observed over the Swiss Plateau and the rain shadow regions of the inner Alps. As durations extend toward 12-24 h, localised peaks are progressively damped, with synoptic-scale processes increasing coherence. For aggregation areas exceeding 100 km², the enhanced rainfall over the alpine barrier weakens and the highest values occur over the Southern Alps.

Event-based analyses of recent significant extreme hydrological events (river floods, flash floods, urban flooding, and debris flows) demonstrate the operational value of this multiscale framework, enabling a direct diagnosis of rainfall event severity across different spatiotemporal scales, directly linking rainfall scaling behaviour to hydrological response. This highlights the necessity of evaluating extremes across multiple dimensions, rather than relying solely on point-scale data.

Future work should extend this IDAF climatology to include transitional and winter periods, although this will require addressing additional challenges related to mixed-phase precipitation and increased radar QPE uncertainty.

https://doi.org/10.5194/egusphere-2026-1800
Preprint. Discussion started: 18 May 2026

Code and data availability

MeteoSwiss has decided to make its data publicly available under open-data. For more information refer to https://www.meteoswiss.admin.ch/services-and-publications/service/open-data.html.

Codes used for the estimation of SMEV parameters and return levels are freely available at https://doi.org/10.5281/zenodo.3971558 (Marra, 2020) and https://doi.org/10.5281/zenodo.7234707 (Marra, 2022)

Author contributions

TR: Conceptualization, Formal analysis, Methodology, Writing – original draft. EM and FM: Conceptualization, Methodology, Writing – review & editing. DW: Data curation. MG: Data curation, Investigation, Writing – review & editing. UG: Investigation, Writing – review & editing.

Competing interests

At least one of the (co-)authors is a member of the editorial board of Hydrology and Earth System Sciences. The authors have no other competing interests to declare.

Acknowledgements.

We thank MeteoSwiss for providing radar and gauge data.

Financial support

This study was supported by the ISF grant no. 1999/22 and the German-Israeli Cooperation in Water Technology Research grant no. 0008963. FM was partially funded by Project “The Geosciences for Sustainable Development” project (Budget Ministero dell'Università e della Ricerca–Dipartimenti di Eccellenza 2023–2027 C93C23002690001).

References

Allamano, P., Claps, P., Laio, F., & Thea, C. (2009). A data-based assessment of the dependence of short-duration precipitation on elevation. Phys. Chem. Earth A/B/C, 34(10–12), 635–641. https://doi.org/10.1016/J.PCE.2009.01.001

Allen, R. J., & DeGaetano, A. T. (2005). Areal Reduction Factors for Two Eastern United States Regions with High Rain-Gauge Density. Journal of Hydrologic Engineering, 10(4), 327–335. https://doi.org/10.1061/(asce)1084-0699(2005)10:4(327)

Asquith, W. H., & Famiglietti, J. S. (2000). Precipitation areal-reduction factor estimation using an annual-maxima centered approach. Journal of Hydrology, 230(1–2), 55–69. https://doi.org/10.1016/S0022-1694(00)00170-0

https://doi.org/10.5194/egusphere-2026-1800
Preprint. Discussion started: 18 May 2026

Avanzi, F., De Michele, C., Gabriele, S., Ghezzi, A., & Rosso, R. (2015). Orographic Signature on Extreme Precipitation of Short Durations. Journal of Hydrometeorology, 16(1), 278–294. https://doi.org/10.1175/JHM-D-14-0063.1

Barton, Y., Giannakaki, P., von Waldow, H., Chevalier, C., Pfahl, S., & Martius, O. (2016). Clustering of regional-scale extreme precipitation events in southern Switzerland. Monthly Weather Review, 144(1), 347–369. https://doi.org/10.1175/MWR-D-15-0205.1

Barton, Y., Sideris, I. V., Raupach, T. H., Gabella, M., Germann, U., & Martius, O. (2020). A multi-year assessment of sub-hourly gridded precipitation for Switzerland based on a blended radar—Rain-gauge dataset. International Journal of Climatology, 40(12), 5208–5222. https://doi.org/10.1002/JOC.6514

Bayabil, H. K., Fares, A., Sharif, H. O., Ghebreyesus, D. T., & Moreno, H. A. (2019). Effects of Spatial and Temporal Data Aggregation on the Performance of the Multi-Radar Multi-Sensor System. JAWRA Journal of the American Water Resources Association, 55(6), 1492–1504. https://doi.org/10.1111/1752-1688.12799

Bell, F. (1976). The areal reduction factor in rainfall frequency estimation. http://nora.nerc.ac.uk/id/eprint/5751/1/IH_035.pdf

Benoit, L., Koch, E., Peleg, N., & Mariethoz, G. (2024). Precipitation-elevation relationship: Non-linearity and space–time variability prevail in the Swiss Alps. Journal of Hydrology X, 25, 100186. https://doi.org/10.1016/j.hydroa.2024.100186

Berne, A., Delrieu, G., Creutin, J.-D., & Obled, C. (2004). Temporal and spatial resolution of rainfall measurements required for urban hydrology. Journal of Hydrology, 299(3–4), 166–179. https://doi.org/10.1016/j.jhydrol.2004.08.002

Beven, K. (2012). Rainfall–Runoff Modelling: The Primer, 2nd ed., Wiley-Blackwell, Chichester, U.K.

Blanchet, J., Ceresetti, D., Molinié, G., & Creutin, J.-D. (2016). A regional GEV scale-invariant framework for intensity duration frequency analysis. Journal of Hydrology, 540, 82–95. https://doi.org/10.1016/j.jhydrol.2016.06.007

Blöschl, G., & Sivapalan, M. (1997). Process controls on regional flood frequency: Coefficient of variation and basin scale. Water Resources Research, 33(12), 2967–2980. https://doi.org/10.1029/97WR00568

Borga, M., Stoffel, M., Marchi, L., Marra, F., & Jakob, M. (2014). Hydrogeomorphic response to extreme rainfall in headwater systems: Flash floods and debris flows. Journal of Hydrology, 518. https://doi.org/10.1016/j.jhydrol.2014.05.022

Bougadis, J., & Adamowski, K. (2006). Scaling model of a rainfall intensity-duration-frequency relationship. Hydrological Processes, 20(17), 3747–3757. https://doi.org/10.1002/hyp.6386

Caldas-Alvarez, A., Feldmann, H., Lucio-Eceiza, E., & Pinto, J. G. (2022). Scale-dependency of extreme precipitation processes in regional climate simulations of the greater Alpine region. https://doi.org/10.5194/wcd-2022-11

Catchlove, R. H., & Ball, J. E. (2003). A hydroinformatic approach to the development of areal reduction factors. 28th Int. Hydrology and Water Resources Symp, 1.9-1.15.

Coles, S. (2001). An Introduction to Statistical Modeling of Extreme Values. https://doi.org/10.1007/978-1-4471-3675-0

Cremonini, R., Voormansik, T., Post, P., & Moisseev, D. (2023). Estimation of extreme precipitation events in Estonia and Italy using dual-polarization weather radar quantitative precipitation estimations. Atmospheric Measurement Techniques, 16(11), 2943–2956. https://doi.org/10.5194/amt-16-2943-2023

https://doi.org/10.5194/egusphere-2026-1800
Preprint. Discussion started: 18 May 2026

Cristiano, E., ten Veldhuis, M.-C., & van de Giesen, N. (2017). Spatial and temporal variability of rainfall and their effects on hydrological response in urban areas – a review. Hydrol. Earth Syst. Sci., 21, 3859–3878. https://doi.org/10.5194/hess-21-3859-2017

Dai, Q., & Han, D. (2014). Exploration of discrepancy between radar and gauge rainfall estimates driven by wind fields. Water Resources Research, 50(10), 8571–8589. https://doi.org/10.1002/2014WR015794

Dallan, E., Borga, M., Fosser, G., Canale, A., Roghani, B., Marani, M., & Marra, F. (2024). A method to assess and explain changes in sub-daily precipitation return levels from convection-permitting simulations. Water Resources Research, 60(5). https://doi.org/10.1029/2023WR035969

De Michele, C., Kottegoda, N. T., & Rosso, R. (2001). The derivation of areal reduction factor of storm rainfall from its scaling properties. Water Resources Research, 37(12), 3247–3252. https://doi.org/10.1029/2001WR000346

Eggert, B., Berg, P., Haerter, J. O., Jacob, D., & Moseley, C. (2015). Temporal and spatial scaling impacts on extreme precipitation. Atmos. Chem. Phys., 15, 5957–5971. https://doi.org/10.5194/acp-15-5957-2015

Falkensteiner, M.-A., Schellander, H., Ehrensperger, G., & Hell, T. (2023). Accounting for seasonality in the metastatistical extreme value distribution. Weather and Climate Extremes, 42. https://doi.org/10.1016/j.wace.2023.100601

Feldmann, M., Hering, A., Gabella, M., & Berne, A. (2023). Hailstorms and rainstorms versus supercells—a regional analysis of convective storm types in the Alpine region. Npj Climate and Atmospheric Science, 6(1), 19. https://doi.org/10.1038/s41612-023-00352-z

FOEN. (2023). Faktenblatt 1: Ausmass und Ursachen der Hochwasser im Juli 2021, Factsheet, Bern, Switzerland (Vol. 2025). https://www.bafu.admin.ch/de/hochwasser-an-den-jurarandseen

Formetta, G., Marra, F., Dallan, E., Zaramella, M., & Borga, M. (2022). Differential orographic impact on sub-hourly, hourly, and daily extreme precipitation. Advances in Water Resources, 159. https://doi.org/10.1016/j.advwatres.2021.104085

Frei, C., & Schär, C. (1998). A precipitation climatology of the Alps from high-resolution rain-gauge observations. International Journal of Climatology, 18(8), 873–900. https://doi.org/10.1002/(SICI)1097-0088(19980630)18:8<873::AID-JOC255>3.0.CO;2-9

Fukutome, S., Liniger, M. A., & Süveges, M. (2015). Automatic threshold and run parameter selection: a climatology for extreme hourly precipitation in Switzerland. Theor Appl Climatol 120, 403–416. https://doi.org/10.1007/s00704-014-1180-5

Gabella, M., Frassl, M., Germann, U., Joerg, P. C., & Wild, E. (2018). UrbanRain18: High-resolution rainfall observations in urban environments. UrbanRain18 11th International Workshop on Precipitation in Urban Areas.

Gabella, M., Wolfensberger, D., Boscacci, M., Grazioli, J., & Germann, U. (2019, September). Dual-polarization radar signatures of the convectively driven Lausanne flash-flood event on June 11, 2018. 39th International Conference on Radar Meteorology.

Germann, U., Boscacci, M., Clementi, L., Gabella, M., Hering, A., Sartori, M., Sideris, I. V., & Calpini, B. (2022). Weather Radar in Complex Orography. Remote Sensing, 14(3), 503. https://doi.org/10.3390/rs14030503

https://doi.org/10.5194/egusphere-2026-1800
Preprint. Discussion started: 18 May 2026

Giannakaki, P., & Martius, O. (2016). Synoptic-scale flow structures associated with extreme precipitation events in northern Switzerland. International Journal of Climatology, 36(6), 2497–2515. https://doi.org/10.1002/joc.4508

Gires, A., Tchiguirinskaia, I., Schertzer, D., Schellart, A., Berne, A., & Lovejoy, S. (2014). Influence of small scale rainfall variability on standard comparison tools between radar and rain gauge data. Atmospheric Research, 138, 125–138. https://doi.org/10.1016/j.atmosres.2013.11.008

Giudicianni, C. (2026). Pseudo multi-scaling model of intensity–duration–frequency (IDF) curves. J. Hydrol., 664, 134370. https://doi.org/10.1016/j.jhydrol.2025.134370

Goudenhoofdt, E., Delobbe, L., & Willems, P. (2017). Regional frequency analysis of extreme rainfall in Belgium based on radar estimates. Hydrol. Earth Syst. Sci., 21, 5385–5399. https://doi.org/10.5194/hess-21-5385-2017

Haruna, A., Blanchet, J., & Favre, A. C. (2022). Performance-based comparison of regionalization methods to improve the at-site estimates of daily precipitation. Hydrol. Earth Syst. Sci, 26. https://doi.org/10.5194/hess-26-2797-2022

Haruna, A., Blanchet, J., & Favre, A. C. (2023). Modeling Intensity-Duration-Frequency Curves for the Whole Range of Non-Zero Precipitation: A Comparison of Models. Water Resources Research, 59(6). https://doi.org/10.1029/2022WR033362

Haruna, A., Blanchet, J., & Favre, A. C. (2024). Estimation of intensity-duration-area-frequency relationships based on the full range of non-zero precipitation from radar-reanalysis data. Water Resources Research, 60(2). https://doi.org/10.1029/2023WR035902

Haruna, A., Blanchet, J., & Favre, A. C. (2025). Joint estimation of trend in bulk and extreme daily precipitation in Switzerland. Weather and Climate Extremes, 48. https://doi.org/10.1016/j.wace.2025.100769

Isotta, F. A., Frei, C., Weilguni, V., Perčec Tadić, M., Lassègues, P., Rudolf, B., Pavan, V., Cacciamani, C., Antolini, G., Ratto, S. M., Munari, M., Micheletti, S., Bonati, V., Lussana, C., Ronchi, C., Panettieri, E., Marigo, G., & Vertačnik, G. (2014). The climate of daily precipitation in the Alps: development and analysis of a high-resolution grid dataset from pan-Alpine rain-gauge data. International Journal of Climatology, 34(5), 1657–1675. https://doi.org/10.1002/joc.3794

Karklinsky, M., & Morin, E. (2006). Spatial characteristics of radar-derived convective rain cells over southern Israel. Meteorologische Zeitschrift, 15(5), 513–520. https://doi.org/10.1127/0941-2948/2006/0153

Keller, D. (2013). Evaluation and comparison of radar-rain gauge combination methods. In Scientific Report MeteoSwiss, (Vol. 94).

Kochendorfer, J., Rasmussen, R., Wolff, M., Baker, B., Hall, M. E., Meyers, T., Landolt, S., Jachcik, A., Isaksen, K., Brækkan, R., & Leeper, R. (2017). The quantification and correction of wind-induced precipitation measurement errors. Hydrol. Earth Syst. Sci., 21, 1973–1989. https://doi.org/10.5194/hess-21-1973-2017

Le Gall, P., Favre, A. C., Naveau, P., & Prieur, C. (2022). Improved Regional Frequency Analysis of rainfall data. Weather and Climate Extremes, 36. https://doi.org/10.1016/j.wace.2022.100456

Lengfeld, K., Kirstetter, P. E., Fowler, H. J., Yu, J., Becker, A., Flamig, Z., & Gourley, J. (2020). Use of radar data for characterizing extreme precipitation at fine scales and short durations. Environmental Research Letters, 15(8), 085003. https://doi.org/10.1088/1748-9326/AB98B4

https://doi.org/10.5194/egusphere-2026-1800
Preprint. Discussion started: 18 May 2026

Lengfeld, K., & Marra, F. (2024). Estimation of design precipitation using weather radar in Germany: A comparison of statistical methods. Journal of Hydrology: Regional Studies, 55, 101952. https://doi.org/10.1016/j.ejrh.2024.101952

Liernur, A. (2023). Added value of high-resolution radar data to study Localized Intense Rain Events (LIRE) in Switzerland [Doctoral research plan]. École Polytechnique Fédérale de Lausanne (EPFL).

Lutz, J., Roksvåg, T., Dyrrdal, A. V, Lussana, C., & Thorarinsdottir, T. L. (2024). Areal reduction factors from gridded data products. J. Hydrol., 635, 131177. https://doi.org/10.1016/j.jhydrol.2024.131177

Marani, M., & Ignaccolo, M. (2015). A metastatistical approach to rainfall extremes. Advances in Water Resources, 79, 121–126. https://doi.org/10.1016/j.advwatres.2015.03.001

Marra, F. (2022). A test for the hypothesis: block maxima are samples from a parent distribution with Weibull tail. Zenodo. https://doi.org/10.5281/zenodo.7234707

Marra, F. (2024). A Unified Framework for Extreme Sub-daily Precipitation Frequency Analyses based on Ordinary Events – data & codes (Version 1.2) [Software]. https://doi.org/10.5281/zenodo.11934843

Marra, F., Amponsah, W., & Papalexiou, S. M. (2023). Non-asymptotic Weibull tails explain the statistics of extreme daily precipitation. Advances in Water Resources, 173, 104388. https://doi.org/10.1016/J.ADVWATRES.2023.104388

Marra, F., Armon, M., Borga, M., & Morin, E. (2021). Orographic Effect on Extreme Precipitation Statistics Peaks at Hourly Time Scales. Geophysical Research Letters, 48(5). https://doi.org/10.1029/2020GL091498

Marra, F., Armon, M., & Morin, E. (2022). Coastal and orographic effects on extreme precipitation revealed by weather radar observations. Hydrology and Earth System Sciences, 26(5), 1439–1458. https://doi.org/10.5194/hess-26-1439-2022

Marra, F., Borga, M., & Morin, E. (2020). A unified framework for extreme subdaily precipitation frequency analyses based on ordinary events. Geophysical Research Letters, 47(18). https://doi.org/10.1029/2020GL090209

Marra, F., Dallan, E., Canale, A., Prosdocimi, I., Papacharalampous, G., Borga, M., & Papalexiou, S. M. (2026). Apparent Heavy Tails of Sub-Daily Precipitation Explained by the Coexistence of Lighter-Tailed Processes. Geophysical Research Letters, 53(2). https://doi.org/10.1029/2025GL119705

Marra, F., Nikolopoulos, E. I., Anagnostou, E. N., & Morin, E. (2018). Metastatistical Extreme Value analysis of hourly rainfall from short records: Estimation of high quantiles and impact of measurement errors. Advances in Water Resources, 117, 27–39. https://doi.org/10.1016/J.ADVWATRES.2018.05.001

Marra, F., Zoccatelli, D., Armon, M., & Morin, E. (2019). A simplified MEV formulation to model extremes emerging from multiple nonstationary underlying processes. Advances in Water Resources, 127, 280–290. https://doi.org/10.1016/j.advwatres.2019.04.002

Mélèse, V., Blanchet, J., & Molinié, G. (2018). Uncertainty estimation of intensity-duration-frequency relationships: A regional analysis. Journal of Hydrology, 558, 579–591. https://doi.org/10.1016/j.jhydrol.2017.07.054

Menabde, M., Seed, A., & Pegram, G. (1999). A simple scaling model for extreme rainfall. Water Resources Research, 35(1), 335–339. https://doi.org/10.1029/1998WR900012

https://doi.org/10.5194/egusphere-2026-1800
Preprint. Discussion started: 18 May 2026

MeteoSwiss. (2018a). Documentation of MeteoSwiss grid-data products. Hourly precipitation estimation through Rain-Gauge and Radar: CombiPrecip. https://www.meteoswiss.admin.ch/dam/jcr:2691db4e-7253-41c6-a413-2c75c9de11e3/ProdDoc_CPC.pdf

MeteoSwiss. (2018b). Klimabulletin Juni 2018. Bundesamt Für Meteorologie Und Klimatologie MeteoSchweiz, 72–86. https://www.meteoswiss.admin.ch/dam/jcr:4a6797eb-80dd-4b72-86ec-bf4b28f2545e/201806_d.pdf

MeteoSwiss. (2024). Rückblick auf die Gewitterlage vom 21. Juni 2024 auf der Alpensüdseite.

Miniussi, A., & Marra, F. (2021). Estimation of extreme daily precipitation return levels at-site and in ungauged locations using the simplified MEV approach. Journal of Hydrology, 603. https://doi.org/10.1016/j.jhydrol.2021.126946

Molnar, P., & Burlando, P. (2008). Variability in the scale properties of high-resolution precipitation data in the Alpine climate of Switzerland. Water Resources Research, 44. https://doi.org/10.1029/2007WR006142

Muchan, K., & Dixon, H. (2019). Insights into rainfall undercatch for differing raingauge rim heights. Hydrology Research, 50(6), 1564–1576. https://doi.org/10.2166/nh.2019.024

Musa, M., Grüter, E., Abbt, M., Häberli, C., Häller, E., Küng, U., Konzelmann, T., & Dössegger, R. (2023). Quality control tools for meteorological data in the MeteoSwiss data warehouse system.

Nhat, L. M., Tachikawa, Y., Sayama, T., & Takara, K. (2007). A Simple Scaling Characteristics of Rainfall in Time and Space to Derive Intensity Duration Frequency Relationships. Proceedings of Hydraulic Engineering, 51, 73–78. https://doi.org/10.2208/prohe.51.73

Nisi, L., Martius, O., Hering, A., Kunz, M., & Germann, U. (2016). Spatial and temporal distribution of hailstorms in the Alpine region: a long-term, high resolution, radar-based analysis. Quarterly Journal of the Royal Meteorological Society, 142(697), 1590–1604. https://doi.org/10.1002/qj.2771

Ochoa-Rodriguez, S., Wang, L.-P., Gires, A., Pina, R. D., Reinoso-Rondinel, R., Bruni, G., Ichiba, A., Gaitan, S., Cristiano, E., van Assel, J., Kroll, S., Murlà-Tuyls, D., Tisserand, B., Schertzer, D., Tchiguirinskaia, I., Onof, C., Willems, P., & ten Veldhuis, M.-C. (2015). Impact of spatial and temporal resolution of rainfall inputs on urban hydrodynamic modelling outputs: A multi-catchment investigation. Journal of Hydrology, 531, 389–407. https://doi.org/10.1016/j.jhydrol.2015.05.035

Overeem, A., Buishand, A., & Holleman, I. (2008). Rainfall depth-duration-frequency curves and their uncertainties. Journal of Hydrology, 348(1–2), 124–134. https://doi.org/10.1016/J.JHYDROL.2007.09.044

Overeem, A., Buishand, T. A., & Holleman, I. (2009). Extreme rainfall analysis and estimation of depth-duration-frequency curves using weather radar. Water Resources Research, 45(10). https://doi.org/10.1029/2009WR007869

Panthou, G., Vischel, T., Lebel, T., Quantin, G., & Molinié, G. (2014). Characterising the space–time structure of rainfall in the Sahel with a view to estimating IDAF curves. Hydrol. Earth Syst. Sci., 18, 5093–5107. https://doi.org/10.5194/hess-18-5093-2014

Panziera, L., Gabella, M., & Germann, U. (2018). A 12-year radar-based climatology of daily and sub-daily extreme precipitation over the Swiss Alps. International Journal of Climatology, 38(10), 3749–3769. https://doi.org/10.1002/joc.5528

https://doi.org/10.5194/egusphere-2026-1800
Preprint. Discussion started: 18 May 2026

Panziera, L., Gabella, M., Zanini, S., Hering, A., Germann, U., & Berne, A. (2016). A radar-based regional extreme rainfall analysis to derive the thresholds for a novel automatic alert system in Switzerland. Hydrol. Earth Syst. Sci., 20, 2317–2332. https://doi.org/10.5194/hess-20-2317-2016

Panziera, L., & Germann, U. (2010). The relation between airflow and Orographic precipitation on the southern side of the Alps as revealed by weather radar. Quarterly Journal of the Royal Meteorological Society, 136(646), 222–238. https://doi.org/10.1002/qj.544

Panziera, L., James, C. N., & Germann, U. (2015). Mesoscale organization and structure of orographic precipitation producing flash floods in the Lago Maggiore region. Quarterly Journal of the Royal Meteorological Society, 141(686), 224–248. https://doi.org/10.1002/qj.2351

Peleg, N., Marra, F., Fatichi, S., Paschalis, A., Molnar, P., & Burlando, P. (2018). Spatial variability of extreme rainfall at radar subpixel scale. Journal of Hydrology, 556, 922–933. https://doi.org/10.1016/J.JHYDROL.2016.05.033

Pollock, M. D., O'Donnell, G., Quinn, P., Dutton, M., Black, A., Wilkinson, M. E., Colli, M., Stagnaro, M., Lanza, L. G., Lewis, E., Kilsby, C. G., & O'Connell, P. E. (2018). Quantifying and Mitigating Wind-Induced Undercatch in Rainfall Measurements. Water Resources Research, 54(6), 3863–3875. https://doi.org/10.1029/2017wr022421

Post, R., & Krajewski, W. F. (2023). Examining the stage-IV radar-rainfall product for Probabilistic rainfall estimation: case study over Iowa. Stochastic Environmental Research and Risk Assessment, 37(9), 3329–3341. https://doi.org/10.1007/s00477-023-02439-8

Ramos, M. H., Creutin, J.-D., & Leblois, E. (2005). Visualization of storm severity. Journal of Hydrology, 315(1–4), 295–307. https://doi.org/10.1016/j.jhydrol.2005.04.007

Rosin, T., Marra, F., & Morin, E. (2024). Exploring patterns in precipitation intensity–duration–area–frequency relationships using weather radar data. Hydrol. Earth Syst. Sci., 28, 3549–3566. https://doi.org/10.5194/hess-28-3549-2024

Saltikoff, E., Lopez, P., Taskinen, A., & Pulkkinen, S. (2015). Comparison of quantitative snowfall estimates from weather radar, rain gauges and a numerical weather prediction model. Boreal Environment Research, 20, 667–678. https://doi.org/10.60910/kzbc-nget

Schleiss, M., Olsson, J., Berg, P., Niemi, T., Kokkonen, T., Thorndahl, S., Nielsen, R., Ellerbæk Nielsen, J., Bozhinova, D., & Pulkkinen, S. (2020). The accuracy of weather radar in heavy rain: A comparative study for Denmark, the Netherlands, Finland and Sweden. Hydrology and Earth System Sciences, 24(6), 3157–3188. https://doi.org/10.5194/HESS-24-3157-2020

Sideris, I. V., Gabella, M., Erdin, R., & Germann, U. (2014). Real-time radar–rain-gauge merging using spatio-temporal co-kriging with external drift in the alpine terrain of Switzerland. Quarterly Journal of the Royal Meteorological Society, 140(680), 1097–1111. https://doi.org/10.1002/qj.2188

Sieck, L. C., Burges, S. J., & Steiner, M. (2007). Challenges in obtaining reliable measurements of point rainfall. Water Resour. Res., 43, W01420. https://doi.org/10.1029/2005WR004519

Svensson, C., & Jones, D. A. (2010). Review of methods for deriving areal reduction factors. Journal of Flood Risk Management, 3(3), 232–245. https://doi.org/10.1111/j.1753-318X.2010.01075.x

https://doi.org/10.5194/egusphere-2026-1800
Preprint. Discussion started: 18 May 2026

Tarasova, L., Basso, S., Zink, M., & Merz, R. (2018). Exploring Controls on Rainfall-Runoff Events: 1. Time Series-Based Event Separation and Temporal Dynamics of Event Runoff Response in Germany. Water Resources Research, 54(10), 7711–7732. https://doi.org/10.1029/2018WR022587

Thomassen, E. D., Thorndahl, S. L., Andersen, C. B., Gregersen, I. B., Arnbjerg-Nielsen, K., & Sørup, H. J. D. (2022). Comparing spatial metrics of extreme precipitation between data from rain gauges, weather radar and high-resolution climate model re-analyses. Journal of Hydrology, 610. https://doi.org/10.1016/j.jhydrol.2022.127915

Thorndahl, S., Einfalt, T., Willems, P., Nielsen, J. E., ten Veldhuis, M.-C., Arnbjerg-Nielsen, K., Rasmussen, M. R., & Molnar, P. (2017). Weather radar rainfall data in urban hydrology. Hydrol. Earth Syst. Sci., 21, 1359–1380. https://doi.org/10.5194/hess-21-1359-2017

Vasiloff, S. V, Howard, K. W., & Zhang, J. (2009). Difficulties with correcting radar rainfall estimates based on rain gauge data: a case study of severe weather in Montana on 16–17 June 2007. Weather Forecast., 24, 1334–1344. https://doi.org/10.1175/2009WAF2222154.1

Vidrio-Sahagún, C. T., & He, J. (2022). Hydrological frequency analysis under nonstationarity using the Metastatistical approach and its simplified version. Advances in Water Resources, 166, 104244. https://doi.org/10.1016/J.ADVWATRES.2022.104244

Villarini, G., Mandapaka, P. V, Krajewski, W. F., & Moore, R. J. (2008). Rainfall and sampling uncertainties: a rain gauge perspective. J. Geophys. Res. Atmos., 113, D11102. https://doi.org/10.1029/2007JD009214

von Matt, C., Stocker, B., & Martius, O. (2025). HYD-RESPONSES: daily hydro-meteorological catchment-level time series to analyse HYDrological drought dynamics in RESPONSE to (cumulative) water deficits in Swiss catchments. Earth System Science Data [Preprint]. https://doi.org/10.5194/essd-2025-383

Wilson, P. S., & Toumi, R. (2005). A fundamental probability distribution for heavy rainfall. Geophysical Research Letters, 32(14), 1–4. https://doi.org/10.1029/2005GL022465

Wolfensberger, D., Gabella, M., Boscacci, M., Germann, U., & Berne, A. (2021). RainForest: a random forest algorithm for quantitative precipitation estimation over Switzerland. Atmospheric Measurement Techniques, 14(4), 3169–3193. https://doi.org/10.5194/AMT-14-3169-2021

Wüest, M., Frei, C., Altenhoff, A., Hagen, M., Litschi, M., & Schär, C. (2010). A gridded hourly precipitation dataset for Switzerland using rain-gauge analysis and radar-based disaggregation. Int. J. Climatol, 1764–1775. https://doi.org/10.1002/joc.2025

Yamoat, N., Hanchoowong, R., Yamoad, O., Chaimoon, N., & Kangrang, A. (2023). Estimation of regional intensity–duration–frequency relationships of extreme rainfall by simple scaling in Thailand. Journal of Water and Climate Change, 14(3), 796–810. https://doi.org/10.2166/WCC.2023.430

Zorzetto, E., Botter, G., & Marani, M. (2016). On the emergence of rainfall extremes from ordinary events. Geophysical Research Letters, 43(15), 8076–8082. https://doi.org/10.1002/2016GL069445